C8166-CCR5 cells retained sensitivity to small-molecule CD4 mimics and sCD4 comparable to that of HIV-1 MNA.

We then examined whether the synergistic neutralization of HIV-1 MNA by KD-247 antibody in the presence of NBD-556 (Yoshimura *et al.*, 2010) would be reproduced when CD4 mimic was substituted by YYA-021. The synergistic neutralization effect of KD-247 and YYA-021 was reproduced in our experiments (Fig. 1d). At 50 μg ml^{-1}, KD-247 barely achieved 50 % neutralization of HIV-1 MNA but resulted in 50 % neutralization at <0.05 μg ml^{-1} in the presence of 20 μM of YYA-021.

Finally, to examine whether these two agents neutralized SHIV MNA in the same manner as the parental HIV-1, we conducted a neutralization assay with KD-247 in the presence of increasing amounts of YYA-021 (0, 5, 10, 20 and 40 μM) (Fig. 1e). The neutralization curve of KD-247 against SHIV MNA showed an upward shift as the concentration of YYA-021 increased (Fig. 1e), similar to the observations with HIV-1 (Fig. 1d), indicating augmentation of neutralization, and complete neutralization of both viruses was achieved at 20 μM YYA-021 (Fig. 1d, e). Based on these results, we concluded that the neutralization profile of SHIV MNA was comparable to that of HIV-1 MNA.

Reproduction of the neutralization characteristics of HIV-1 MNA in the newly generated SHIV prompted us to assess the ability of SHIV MNA to replicate in monkey cells. SHIV MNA, along with SIV239 and SHIV KS661, were normalized with infectious titres and inoculated into rhesus macaque PBMC preparations from four animals,

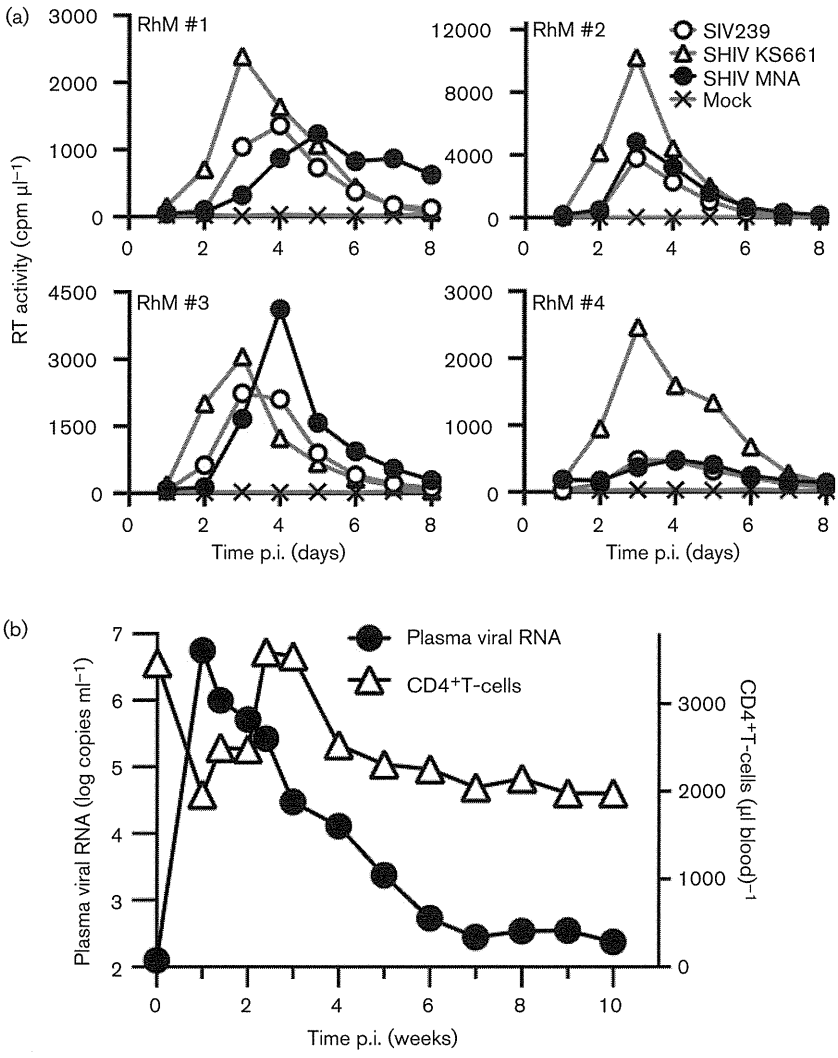

Fig. 2. Replication of SHIV MNA in rhesus macaque PBMCs (a) and *in vivo* (b). (a) M.o.i. was adjusted to 0.01 ($TCID_{50}$ per cell). (b) Experimental infection of a rhesus macaque with SHIV MNA. SHIV MNA (1.75×10^5 $TCID_{50}$) was intravenously inoculated into a rhesus macaque, and the plasma viral RNA burden and circulating $CD4^+$ T-lymphocytes were monitored.

as described previously (Fujita *et al.*, 2013) (Fig. 2a). SHIV KS661, a CXCR4-utilizing virus, replicated to the highest titres of all the viruses in all PBMC preparations. Compared with SHIV KS661, SIV239 replicated to lower titres. Under these experimental conditions, SHIV MNA showed productive replication in the cells with similar replication kinetics and peak titres to SIV239. Based on these results, we concluded that SHIV MNA was replication competent in primary monkey lymphocytes.

Productive replication of SHIV MNA in monkey PBMCs justified experimental infection of the virus *in vivo*. We inoculated 1.75×10^5 $TCID_{50}$ SHIV MNA intravenously into a rhesus macaque and monitored plasma viral RNA burden and circulating $CD4^+$ T-lymphocyte levels (Fig. 2b). Plasma viral RNA burden reached a peak of 5.6×10^6 copies ml^{-1} at 1 week post-infection (p.i.), and declined rapidly thereafter, reaching low levels of detection at 7 weeks p.i. (around 2.8×10^2 copies ml^{-1}). Circulating $CD4^+$ T-cell numbers showed a transient decrease around 1 week p.i., rebounded around 3 weeks p.i. and stabilized around 70 % of the pre-infection level from 4 weeks p.i. During the period of observation, the animal developed no obvious clinical manifestations related to lentivirus infection.

As SHIV MNA replicated *in vivo* without depleting helper T-cells, it was expected that the animal mounted an antiviral immune reaction. The production of antibody directed against Env was assessed by Western blotting, as described previously (Igarashi *et al.*, 1999). Purified Env protein (Advanced Biotechnologies) was used as the antigen (Fig. 3a). Anti-Env antibody was detected at 3 weeks p.i., and the level of antibody judged by the intensity of the band increased gradually with time.

We next examined whether the animal generated neutralizing antibodies against SHIV MNA. Because plasma samples from this specimen exhibited high background activity, IgG was purified from these samples collected on day 0 and in week 24 p.i. using protein G spin columns (GE Healthcare Japan). While the IgG from day 0 exhibited no neutralizing activity (Fig. 3b), as expected, the IgG collected at 24 weeks p.i. neutralized SHIV MNA, although a concentration >100 μg ml^{-1} was required to suppress replication of 100 $TCID_{50}$ of the input virus (Fig. 3c).

We examined whether the observed marginal neutralization by the antibody could be enhanced by the presence of YYA-021. Upon addition of YYA-021 in the assay system, SHIV MNA became sensitive to IgG obtained at 24 weeks p.i. (Fig. 3c), while no enhancement was identified from day 0 (Fig. 3b).

In this study, we generated a replication-competent SHIV MNA strain carrying an Env resistant to the neutralizing mAb KD-247 but conditionally sensitive in the presence of the CD4 mimic YYA-021. As the observed neutralization characteristics were identical to those of HIV-1 MNA, which contributed the majority of the Env sequence to the chimaera, the utility of the CD4 mimic as a means of enhancing antibody-mediated virus neutralization should be assessed in the context of infection *in vivo*. This concept could be tested during the acute phase of SHIV MNA infection, during which the virus undergoes substantial replication. To examine the feasibility of CD4-mimic-mediated enhancement of virus neutralization in the context of chronic infection, the conditions under which this type of intervention should be applied to HIV-1-infected patients in a clinical setting, the virus must be

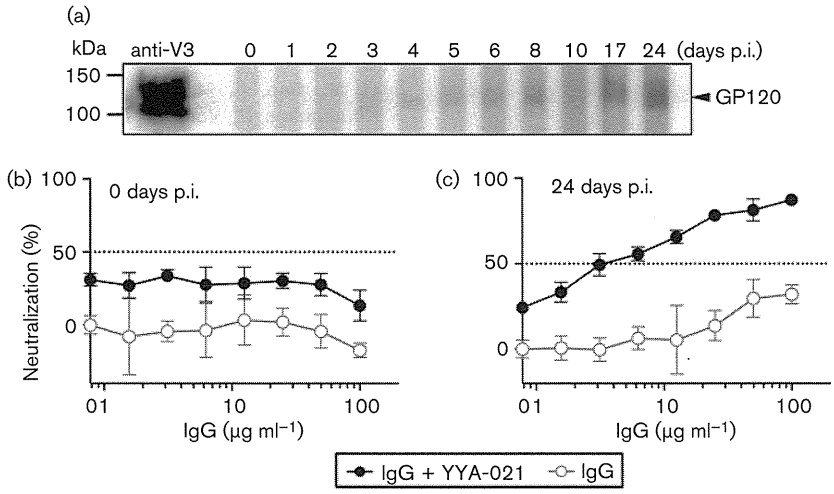

Fig. 3. Antibody induced against SHIV MNA. (a) The anti-HIV-1 gp120 antibody response was assessed by Western blotting with plasma samples collected at the indicated times. An anti-HIV-1 V3 mAb, 4G10 (ascites diluted 1 : 100) (von Brunn *et al.*, 1993), obtained from the NIH AIDS Reagent Program, was used as a positive control (lane anti-V3). (b, c) Neutralization of SHIV MNA with IgG purified from plasma of the infected rhesus macaque (day 0 and week 24 p.i.) with 20 μM YYA-021 or without YYA-021.

modified to sustain productive replication for a longer period. SHIV MNA in the present form does not fulfil this requirement. It is possible that animal-to-animal passage could increase the fitness of the virus in monkeys.

This study demonstrated that a CD4 mimic could modulate viral Env protein to be more susceptible to neutralization by less potent antibodies generated in the context of infection. During the early phase of infection, patients mount high titres of non-neutralizing antibodies directed against the V3 loop (Davis *et al.*, 2009a). Patients with HIV-1 clade C generate anti-Env antibodies, including anti-CD4i antibodies, with poor neutralizing activity against recent infection (Gray *et al.*, 2007). It is possible that the CD4 mimic YYA-021 causes a conformational change in SHIV MNA Env, which renders sequestered epitope(s) accessible to potentially neutralizing IgG, such as ones directed against the V3 loop and CD4i.

The current study extended the previous study by Yoshimura *et al.* (2010) and used HIV-1 MNA belonging to clade B to generate a new SHIV strain carrying Env. The neutralization sensitivity of this strain is characteristically augmented in the presence of a small-molecule CD4 mimic. Similar observations by Decker *et al.* (2005) showed that infections of a wide range of HIV-1 strains of multiple clades or circulating recombinant forms elicit high titres of anti-CD4i antibodies. These anti-CD4i antibodies neutralize viruses as divergent as HIV-2 in the presence of sCD4 (Decker *et al.*, 2005). Taking these observations into account, small-molecule CD4 mimics such as YYA-021 could potentially enhance the neutralization activity of the antibodies directed against autologous viruses belonging not only to clade B but also to multiple HIV-1 strains of various clades and possibly even HIV-2. Our results pave the way for a novel therapeutic intervention based on administration of CD4 mimics to patients with HIV to facilitate control of the virus by their own antibodies.

Acknowledgements

Thanks should be given to: Drs Julie Strizki and Paul Zavodny of the Schering-Plough Research Institute, Kenilworth, NJ, USA, for providing AD101; the NIH AIDS Research & Reference Reagent Program for providing TZM-bl cells, SV-A-MLV-env, 4G10 and soluble CD4; the Chemo-Sero-Therapeutic Research Institute, Kaketsuken, Japan, for providing mAb KD-247; former and current members of the Igarashi Laboratory for discussion and support. This work was supported by a Research on HIV/AIDS grant from the Ministry of Health, Labor and Welfare of Japan (H22-AIDS Research-007 and H24-AIDS Research-008) and by a Grant-in-Aid for Scientific Research (B) from the Japan Society for the Promotion of Science (23300156).

References

Davis, K. L., Bibollet-Ruche, F., Li, H., Decker, J. M., Kutsch, O., Morris, L., Salomon, A., Pinter, A., Hoxie, J. A. & other authors (2009a). Human immunodeficiency virus type 2 (HIV-2)/HIV-1 envelope chimeras detect high titers of broadly reactive HIV-1 V3-specific antibodies in human plasma. *J Virol* **83**, 1240–1259.

Davis, K. L., Gray, E. S., Moore, P. L., Decker, J. M., Salomon, A., Montefiori, D. C., Graham, B. S., Keefer, M. C., Pinter, A. & other authors (2009b). High titer HIV-1 V3-specific antibodies with broad reactivity but low neutralizing potency in acute infection and following vaccination. *Virology* **387**, 414–426.

Decker, J. M., Bibollet-Ruche, F., Wei, X., Wang, S., Levy, D. N., Wang, W., Delaporte, E., Peeters, M., Derdeyn, C. A. & other authors (2005). Antigenic conservation and immunogenicity of the HIV coreceptor binding site. *J Exp Med* **201**, 1407–1419.

Eda, Y., Takizawa, M., Murakami, T., Maeda, H., Kimachi, K., Yonemura, H., Koyanagi, S., Shiosaki, K., Higuchi, H. & other authors (2006). Sequential immunization with V3 peptides from primary human immunodeficiency virus type 1 produces cross-neutralizing antibodies against primary isolates with a matching narrow-neutralization sequence motif. *J Virol* **80**, 5552–5562.

Fujita, Y., Otsuki, H., Watanabe, Y., Yasui, M., Kobayashi, T., Miura, T. & Igarashi, T. (2013). Generation of a replication-competent chimeric simian-human immunodeficiency virus carrying env from subtype C clinical isolate through intracellular homologous recombination. *Virology* **436**, 100–111.

Gray, E. S., Moore, P. L., Choge, I. A., Decker, J. M., Bibollet-Ruche, F., Li, H., Leseka, N., Treurnicht, F., Mlisana, K. & other authors (2007). Neutralizing antibody responses in acute human immunodeficiency virus type 1 subtype C infection. *J Virol* **81**, 6187–6196.

Igarashi, T., Endo, Y., Englund, G., Sadjadpour, R., Matano, T., Buckler, C., Buckler-White, A., Plishka, R., Theodore, T. & other authors (1999). Emergence of a highly pathogenic simian/human immunodeficiency virus in a rhesus macaque treated with anti-CD8 mAb during a primary infection with a nonpathogenic virus. *Proc Natl Acad Sci U S A* **96**, 14049–14054.

Kong, L. & Sattentau, Q. J. (2012). Antigenicity and immunogenicity in HIV-1 antibody-based vaccine design. *J AIDS Clin Res* **S8**, 3.

Kwong, P. D. & Mascola, J. R. (2012). Human antibodies that neutralize HIV-1: identification, structures, and B cell ontogenies. *Immunity* **37**, 412–425.

Landau, N. R., Page, K. A. & Littman, D. R. (1991). Pseudotyping with human T-cell leukemia virus type I broadens the human immunodeficiency virus host range. *J Virol* **65**, 162–169.

Li, M., Gao, F., Mascola, J. R., Stamatatos, L., Polonis, V. R., Koutsoukos, M., Voss, G., Goepfert, P., Gilbert, P. & other authors (2005). Human immunodeficiency virus type 1 *env* clones from acute and early subtype B infections for standardized assessments of vaccine-elicited neutralizing antibodies. *J Virol* **79**, 10108–10125.

Lusso, P., Earl, P. L., Sironi, F., Santoro, F., Ripamonti, C., Scarlatti, G., Longhi, R., Berger, E. A. & Burastero, S. E. (2005). Cryptic nature of a conserved, CD4-inducible V3 loop neutralization epitope in the native envelope glycoprotein oligomer of CCR5-restricted, but not CXCR4-using, primary human immunodeficiency virus type 1 strains. *J Virol* **79**, 6957–6968.

Madani, N., Schön, A., Princiotto, A. M., Lalonde, J. M., Courter, J. R., Soeta, T., Ng, D., Wang, L., Brower, E. T. & other authors (2008). Small-molecule CD4 mimics interact with a highly conserved pocket on HIV-1 gp120. *Structure* **16**, 1689–1701.

Mascola, J. R., Stiegler, G., VanCott, T. C., Katinger, H., Carpenter, C. B., Hanson, C. E., Beary, H., Hayes, D., Frankel, S. S. & other authors (2000). Protection of macaques against vaginal transmission of a pathogenic HIV-1/SIV chimeric virus by passive infusion of neutralizing antibodies. *Nat Med* **6**, 207–210.

Moore, J. P., Cao, Y., Qing, L., Sattentau, Q. J., Pyati, J., Koduri, R., Robinson, J., Barbas, C. F., III, Burton, D. R. & Ho, D. D. (1995).

Primary isolates of human immunodeficiency virus type 1 are relatively resistant to neutralization by monoclonal antibodies to gp120, and their neutralization is not predicted by studies with monomeric gp120. *J Virol* **69**, 101–109.

Narumi, T., Ochiai, C., Yoshimura, K., Harada, S., Tanaka, T., Nomura, W., Arai, H., Ozaki, T., Ohashi, N. & other authors (2010). CD4 mimics targeting the HIV entry mechanism and their hybrid molecules with a CXCR4 antagonist. *Bioorg Med Chem Lett* **20**, 5853–5858.

Narumi, T., Arai, H., Yoshimura, K., Harada, S., Nomura, W., Matsushita, S. & Tamamura, H. (2011). Small molecular CD4 mimics as HIV entry inhibitors. *Bioorg Med Chem* **19**, 6735–6742.

Narumi, T., Arai, H., Yoshimura, K., Harada, S., Hirota, Y., Ohashi, N., Hashimoto, C., Nomura, W., Matsushita, S. & Tamamura, H. (2013). CD4 mimics as HIV entry inhibitors: lead optimization studies of the aromatic substituents. *Bioorg Med Chem* **21**, 2518–2526.

Nishimura, Y., Igarashi, T., Haigwood, N. L., Sadjadpour, R., Donau, O. K., Buckler, C., Plishka, R. J., Buckler-White, A. & Martin, M. A. (2003). Transfer of neutralizing IgG to macaques 6 h but not 24 h after SHIV infection confers sterilizing protection: implications for HIV-1 vaccine development. *Proc Natl Acad Sci U S A* **100**, 15131–15136.

Nishimura, Y., Shingai, M., Willey, R., Sadjadpour, R., Lee, W. R., Brown, C. R., Brenchley, J. M., Buckler-White, A., Petros, R. & other authors (2010). Generation of the pathogenic R5-tropic simian/human immunodeficiency virus SHIVAD8 by serial passaging in rhesus macaques. *J Virol* **84**, 4769–4781.

Platt, E. J., Wehrly, K., Kuhmann, S. E., Chesebro, B. & Kabat, D. (1998). Effects of CCR5 and CD4 cell surface concentrations on infections by macrophagetropic isolates of human immunodeficiency virus type 1. *J Virol* **72**, 2855–2864.

Shibata, R. & Adachi, A. (1992). SIV/HIV recombinants and their use in studying biological properties. *AIDS Res Hum Retroviruses* **8**, 403–409.

Shimizu, Y., Okoba, M., Yamazaki, N., Goto, Y., Miura, T., Hayami, M., Hoshino, H. & Haga, T. (2006). Construction and in vitro characterization of a chimeric simian and human immunodeficiency virus with the RANTES gene. *Microbes Infect* **8**, 105–113.

Shinohara, K., Sakai, K., Ando, S., Ami, Y., Yoshino, N., Takahashi, E., Someya, K., Suzaki, Y., Nakasone, T. & other authors (1999). A highly pathogenic simian/human immunodeficiency virus with genetic changes in cynomolgus monkey. *J Gen Virol* **80**, 1231–1240.

Thali, M., Moore, J. P., Furman, C., Charles, M., Ho, D. D., Robinson, J. & Sodroski, J. (1993). Characterization of conserved human immunodeficiency virus type 1 gp120 neutralization epitopes exposed upon gp120-CD4 binding. *J Virol* **67**, 3978–3988.

von Brunn, A., Brand, M., Reichhuber, C., Morys-Wortmann, C., Deinhardt, F. & Schödel, F. (1993). Principal neutralizing domain of HIV-1 is highly immunogenic when expressed on the surface of hepatitis B core particles. *Vaccine* **11**, 817–824.

Wei, X., Decker, J. M., Liu, H., Zhang, Z., Arani, R. B., Kilby, J. M., Saag, M. S., Wu, X., Shaw, G. M. & Kappes, J. C. (2002). Emergence of resistant human immunodeficiency virus type 1 in patients receiving fusion inhibitor (T-20) monotherapy. *Antimicrob Agents Chemother* **46**, 1896–1905.

Wyatt, R., Kwong, P. D., Desjardins, E., Sweet, R. W., Robinson, J., Hendrickson, W. A. & Sodroski, J. G. (1998). The antigenic structure of the HIV gp120 envelope glycoprotein. *Nature* **393**, 705–711.

Yamada, Y., Ochiai, C., Yoshimura, K., Tanaka, T., Ohashi, N., Narumi, T., Nomura, W., Harada, S., Matsushita, S. & Tamamura, H. (2010). CD4 mimics targeting the mechanism of HIV entry. *Bioorg Med Chem Lett* **20**, 354–358.

Yoshimura, K., Harada, S., Shibata, J., Hatada, M., Yamada, Y., Ochiai, C., Tamamura, H. & Matsushita, S. (2010). Enhanced exposure of human immunodeficiency virus type 1 primary isolate neutralization epitopes through binding of CD4 mimetic compounds. *J Virol* **84**, 7558–7568.

Yusa, K., Maeda, Y., Fujioka, A., Monde, K. & Harada, S. (2005). Isolation of TAK-779-resistant HIV-1 from an R5 HIV-1 GP120 V3 loop library. *J Biol Chem* **280**, 30083–30090.

Zhao, Q., Ma, L., Jiang, S., Lu, H., Liu, S., He, Y., Strick, N., Neamati, N. & Debnath, A. K. (2005). Identification of *N*-phenyl-*N'*-(2,2,6,6-tetramethyl-piperidin-4-yl)-oxalamides as a new class of HIV-1 entry inhibitors that prevent gp120 binding to CD4. *Virology* **339**, 213–225.

LETTER TO THE EDITOR

EFdA, a Reverse Transcriptase Inhibitor, Potently Blocks HIV-1 *Ex Vivo* Infection of Langerhans Cells within Epithelium

Journal of Investigative Dermatology advance online publication, 2 January 2014; doi:10.1038/jid.2013.467

TO THE EDITOR

Despite increasing access to antiretroviral drugs, sexual transmission of HIV-1 remains a significant public health threat. A recent clinical trial, CAPRISA 004, of a vaginally administered microbicide using a nucleoside reverse transcriptase inhibitor (NRTI), tenofovir (TDF), has demonstrated that 1% TDF gel reduced HIV-1 acquisition by an estimated 39% overall (Abdool Karim *et al.*, 2010), indicating a potential utility of NRTI-based microbicides. In the VOICE study, however, a once-daily dosing regimen with TDF gel failed to demonstrate protective effects in at-risk women. These studies demonstrate the need to develop additional more potent microbicide candidates to potentially increase the activity to protect women from HIV-1 transmission.

We previously reported that a series of 4′-substituted NRTIs have excellent antiviral properties (Ohrui, 2006), and through optimization of such 4′-substituted NRTIs, 4′-ethynyl-2-fluoro-2′-deoxyadenosine (EFdA) was found to exert extremely potent activity against a wide spectrum of HIV-1 strains including highly multidrug-resistant clinical HIV-1 isolates, with favorable *in vitro* cell toxicities (Nakata *et al.*, 2007; Ohrui *et al.*, 2007). EFdA inhibited HIV-1 replication in activated peripheral blood mononuclear cells with an EC_{50} of 0.05 nM, a potency several orders of magnitude greater than any of the current clinically available NRTIs (Michailidis *et al.*, 2009). As the prevalence of new infections with drug-resistant HIV-1 variants could increase in the coming years (Nichols *et al.*, 2011), EFdA may be useful as a topical microbicide.

Langerhans cells (LCs) are dendritic cells located, among other sites, within genital skin and mucosal epithelium (Lederman *et al.*, 2006). In female rhesus macaques exposed intravaginally to simian immunodeficiency virus, up to 90% of initially infected target cells were LCs (Hu *et al.*, 2000). *Ex vivo* experiments with human foreskin explants show that epidermal LCs in inner foreskin are primary target cells for HIV-1 infection, providing a plausible explanation for why circumcision greatly reduces the probability of acquiring HIV-1 (Ganor *et al.*, 2010; Zhou *et al.*, 2011). LCs also express CD4 and CCR5, but not CXCR4, and demonstrate the distinctive characteristics of emigrating from tissue to draining lymph nodes in order to interact with T cells following contact with pathogens (Lederman *et al.*, 2006). Indeed, epidermal LCs are readily infected *ex vivo* with R5-HIV-1, but not with X4-HIV-1, and initiate and promote high levels of infection upon interactions with cocultured $CD4^+$ T cells (Kawamura *et al.*, 2000; Ogawa *et al.*, 2009, 2013), consistent with previous epidemiologic observations that the majority of HIV-1 strains isolated from newly infected patients are R5-HIV-1 strains (Zhu *et al.*, 1993). Thus, LCs likely have an important role in disseminating HIV-1 soon after exposure to the virus.

To understand how HIV-1 traverses skin and genital mucosa, an *ex vivo* model was developed in which resident LCs within epithelial tissue explants obtained from suction blisters are exposed to HIV-1 and then allowed to emigrate from the tissue, thus mimicking conditions that occur following mucosal exposure to HIV (Kawamura *et al.*, 2000; Ogawa *et al.*, 2009, 2013). In this model, although relatively few productively infected LCs are identified, these cells induce high levels of HIV-1 infection when cocultured with resting autologous $CD4^+$ T cells (Kawamura *et al.*, 2000; Ogawa *et al.*, 2013). As expected, when epidermal tissue explants were pretreated with various concentrations of TDF, EFdA, and CCR5 inhibitor, maraviroc (MVC), prior to R5-tropic $HIV\text{-}1_{Ba\text{-}L}$ exposure, HIV-1 infection of resident LCs within epidermis as well as subsequent virus transmission from emigrated LCs to cocultured $CD4^+$ T cells was decreased in a dose-dependent manner (Figure 1a and c; for detailed methods, see Supplementary Material). The blocking was confirmed by repeated experiments using skin explants from three additional randomly selected individuals (Figure 1b and d). Strikingly, although the blocking efficiency of TDF or MVC even at 5,000 nM was partial, EFdA demonstrated complete blocking of R5-HIV-1 replication in LCs as well as subsequent virus transmission from emigrated LCs to $CD4^+$ T cells at doses of 100–5,000 nM (Figure 1a–d). Furthermore, EFdA blocked *ex vivo* virus infection of LCs as well as subsequent virus transmission when two strains of R5-HIV-1, $HIV\text{-}1_{JR\text{-}FL}$ and $HIV\text{-}1_{AD8}$, were utilized in experiments ($n=3$, Supplementary Figure S1 online).

Similar to the results in epidermal LCs, preincubation of monocyte-derived LCs (mLCs) with 100–5,000 nM of EFdA

Abbreviations: EFdA, 4′-ethynyl-2-fluoro-2′-deoxyadenosine; LC, Langerhans cell; mLC, monocyte-derived LC; MVC, maraviroc; NRTI, nucleoside reverse transcriptase inhibitor; TDF, tenofovir

Accepted article preview online 11 November 2013

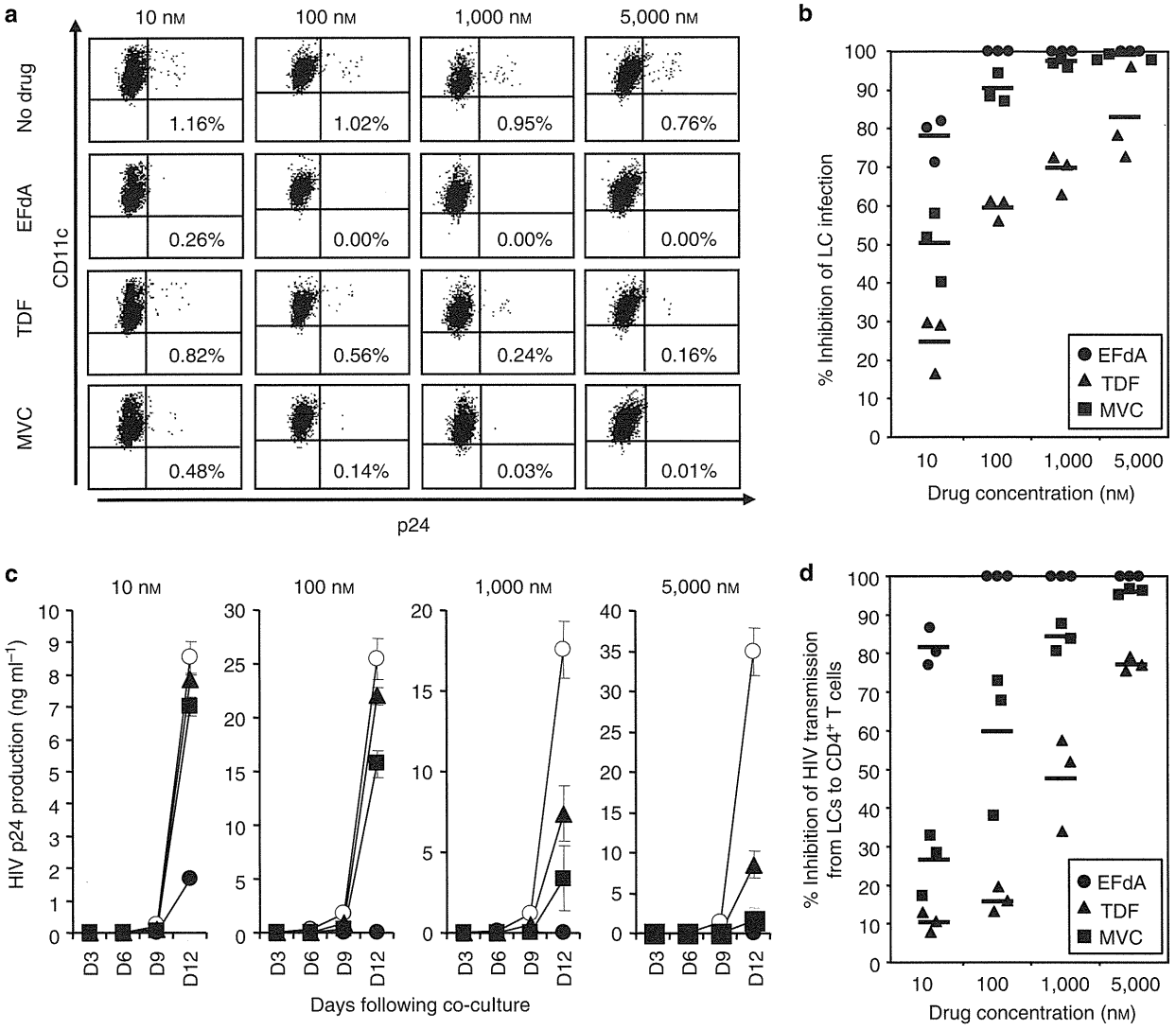

Figure 1. Preincubation of skin explants with EFdA blocks R5-HIV-1 infection in LCs and subsequent virus transmission to cocultured CD4$^+$ T cells. LCs within skin explants were preincubated with no drug (○) or the indicated concentrations of EFdA (●), TDF (▲), and MVC (■) for 30 minutes, exposed to HIV-1_{Ba-L} for 2 hours, and then floated on culture medium to allow migration of LCs from the explants. Emigrating cells from the epidermal sheets were collected 3 days following HIV-1 exposure. HIV-1-infected LCs were assessed by HIV-1 p24 intracellular staining in langerin$^+$ CD11c$^+$ LCs (**a**, **b**), or further cocultured with autologous CD4$^+$ T cells and culture supernatants were assessed for p24 content by ELISA on the indicated days (**c**, **d**). Summary of percent inhibition of LC infection (**b**) and virus transmission to CD4$^+$ T cells (**d**) of 12 experiments using skin explants from 12 individuals with the indicated each concentration of EFdA (●), TDF (▲), and MVC (■) are shown. Mean values obtained from different donors are shown as horizontal marks (**b**, **d**). EFdA, 4′-ethynyl-2-fluoro-2′-deoxyadenosine; LCs, Langerhans cells; MVC, maraviroc; TDF, tenofovir.

completely blocked HIV-1 replication in mLCs as well as subsequent virus transmission from mLCs to cocultured CD4$^+$ T cells, whereas both TDF and MVC at the same doses only partially inhibited the transmission (Figure 2a and b; for detailed methods, see Supplementary Material online). Intriguingly, even in 1–3 days following the removal of EFdA (1,000 nM), EFdA completely blocked HIV-1 infection of mLCs as well as subsequent virus transmission from mLCs to cocultured CD4$^+$ T cells, whereas TDF and MVC rapidly lost their anti-HIV-1 activity within days (Figure 2c–f). No cellular toxicity was noted for any of these drugs at the doses used in these experiments (Supplementary Figure S2 online). When similar experiments were conducted using peripheral blood mononuclear cell as target cells, virtually identical favorable persistency of EFdA in antiviral activity compared with that of TDF was observed (data not shown).

In the present work, we demonstrated that EFdA exerted extremely more potent anti-HIV-1 activity in LCs than did TDF and MVC, and the potent anti-HIV-1 activity of EFdA persisted for at least 3 days. Of note, the efficacy of TDF gel in CAPRISA 004 has been linked to its long intracellular half-life (Abdool Karim *et al.*, 2010; Rohan *et al.*, 2010). Our data strongly

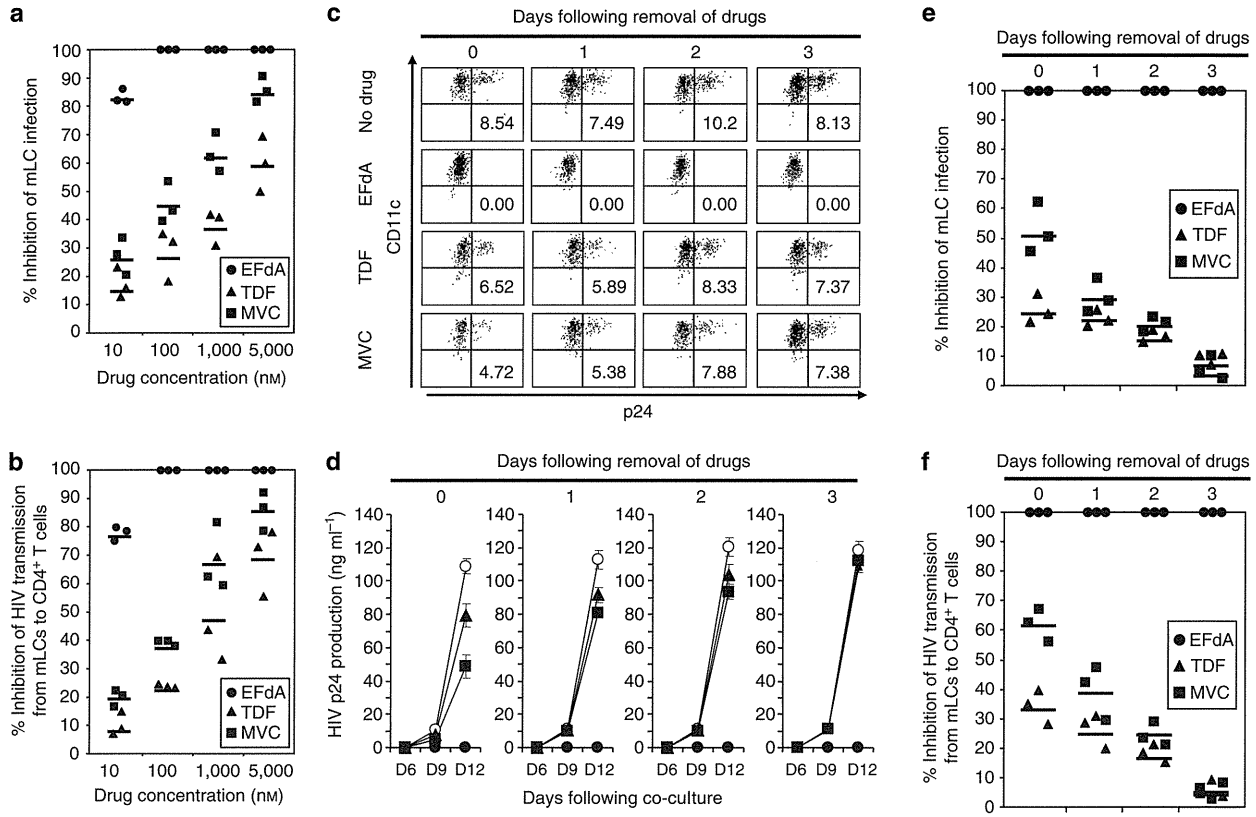

Figure 2. Preincubation of skin explants with EFdA blocks subsequent R5-HIV-1 infection in LC in a dose-dependent manner. mLCs were preincubated with no drug (○) or the indicated concentrations of EFdA (●), TDF (▲) and MVC (■) for 30 minutes, and then immediately exposed to HIV-1Ba-L for 2 hours (**a**, **b**), or thoroughly washed to remove the extracellular drug and further cultured for 1, 2, or 3 days prior to exposure to HIV-1Ba-L for 2 hours (**c**–**f**). After 7 days of HIV-1 exposure, HIV-1-infected mLCs were assessed by HIV-1 p24 intracellular staining in langerin$^+$ CD11c$^+$ mLCs (**a**, **c**, **e**), or further cocultured with autologous CD4$^+$ T cells and culture supernatants were assessed for p24 content by ELISA on the indicated days (**b**, **d**, **f**). Summary of percent inhibition of mLC infection (**a**, **e**) and virus transmission to CD4$^+$ T cells (**b**, **f**) of three independent experiments are shown. Mean values are shown as horizontal marks (**a**, **b**, **e**, **f**). EFdA, 4′-ethynyl-2-fluoro-2′-deoxyadenosine; LCs, Langerhans cells; mLCs, monocyte-derived LCs; MVC, maraviroc; TDF, tenofovir.

indicate that EFdA may serve as a promising microbicide to block sexual transmission of HIV-1 because of its potent anti-HIV-1 activity, low cytotoxicity, and superior persistence of antiviral activity against HIV-1 in LCs.

CONFLICT OF INTEREST

HM is among coinventors on a patent for EFdA; all rights, title, and interest to the patent have been assigned to Yamasa Corporation, Chiba, Japan. The other authors state no conflict of interest.

ACKNOWLEDGMENTS

Financial support was provided by the Ministry of Health Science of the Japanese Government (201029002), the Intramural Research Program of Center for Cancer Research, National Cancer Institute, National Institutes of Health, and a grant for global education and research center aiming at the control of AIDS (Global Center of Excellence supported by Monbu-Kagakusho).

Takamitsu Matsuzawa[1], Tatsuyoshi Kawamura[1], Youichi Ogawa[1], Kenji Maeda[2], Hirotomo Nakata[3], Kohji Moriishi[4], Yoshio Koyanagi[5], Hiroyuki Gatanaga[6], Shinji Shimada[1] and Hiroaki Mitsuya[2,3]

[1]Faculty of Medicine, Department of Dermatology, University of Yamanashi, Yamanashi, Japan; [2]Experimental Retrovirology Section, HIV and AIDS Malignancy Branch, National Cancer Institute, National Institutes of Health, Bethesda, Maryland, USA; [3]Department of Infectious Diseases and Hematology, Kumamoto University School of Medicine, Kumamoto, Japan; [4]Faculty of Medicine, Department of Microbiology, University of Yamanashi, Yamanashi, Japan; [5]Laboratory of Viral Pathogenesis, Institute for Virus Research, Kyoto University, Kyoto, Japan and [6]AIDS Clinical Center, National Center for Global Health and Medicine, Tokyo, Japan
E-mail: tkawa@yamanashi.ac.jp

SUPPLEMENTARY MATERIAL

Supplementary material is linked to the online version of the paper at http://www.nature.com/jid

REFERENCES

Abdool Karim Q, Abdool Karim SS, Frohlich JA *et al.* (2010) Effectiveness and safety of tenofovir gel, an antiretroviral microbicide, for the prevention of HIV infection in women. *Science* 329:1168–74

Ganor Y, Zhou Z, Tudor D *et al.* (2010) Within 1 h, HIV-1 uses viral synapses to enter efficiently the inner, but not outer, foreskin mucosa and engages Langerhans-T cell conjugates. *Mucosal Immunol* 3:506–22

Hu J, Gardner MB, Miller CJ (2000) Simian immunodeficiency virus rapidly penetrates the cervicovaginal mucosa after intravaginal inoculation and infects intraepithelial dendritic cells. *J Virol* 74:6087–95

Kawamura T, Cohen SS, Borris DL *et al.* (2000) Candidate microbicides block HIV-1 infection of human immature Langerhans cells within

epithelial tissue explants. *J Exp Med* 192: 1491–500

Lederman MM, Offord RE, Hartley O (2006) Microbicides and other topical strategies to prevent vaginal transmission of HIV. *Nat Rev Immunol* 6:371–82

Michailidis E, Marchand B, Kodama EN *et al.* (2009) Mechanism of inhibition of HIV-1 reverse transcriptase by 4′-Ethynyl-2-fluoro-2′-deoxyadenosine triphosphate, a translocation-defective reverse transcriptase inhibitor. *J Biol Chem* 284:35681–91

Nakata H, Amano M, Koh Y *et al.* (2007) Activity against human immunodeficiency virus type 1, intracellular metabolism, and effects on human DNA polymerases of 4′-ethynyl-2-fluoro-2′-deoxyadenosine. *Antimicrob Agents Chemother* 51:2701–8

Nichols BE, Boucher CA, van de Vijver DA (2011) HIV testing and antiretroviral treatment strategies for prevention of HIV infection: impact on antiretroviral drug resistance. *J Intern Med* 270:532–49

Ogawa Y, Kawamura T, Kimura T *et al.* (2009) Gram-positive bacteria enhance HIV-1 susceptibility in Langerhans cells, but not in dendritic cells, via Toll-like receptor activation. *Blood* 113:5157–66

Ogawa Y, Kawamura T, Matsuzawa T *et al.* (2013) Antimicrobial peptide LL-37 produced by HSV-2-infected keratinocytes enhances HIV infection of Langerhans cells. *Cell Host Microbe* 13:77–86

Ohrui H (2006) 2′-deoxy-4′-C-ethynyl-2-fluoro-adenosine, a nucleoside reverse transcriptase inhibitor, is highly potent against all human immunodeficiency viruses type 1 and has low toxicity. *Chem Rec* 6:133–43

Ohrui H, Kohgo S, Hayakawa H *et al.* (2007) 2′-Deoxy-4′-C-ethynyl-2-fluoroadenosine: a nucleoside reverse transcriptase inhibitor with highly potent activity against wide spectrum of HIV-1 strains, favorable toxic profiles, and stability in plasma. *Nucleosides, Nucleotides Nucleic Acids* 26: 1543–6

Rohan LC, Moncla BJ, Kunjara Na Ayudhya RP *et al.* (2010) *In vitro* and *ex vivo* testing of tenofovir shows it is effective as an HIV-1 microbicide. *PLoS One* 5:e9310

Zhou Z, Barry de Longchamps N, Schmitt A *et al.* (2011) HIV-1 efficient entry in inner foreskin is mediated by elevated CCL5/RANTES that recruits T cells and fuels conjugate formation with Langerhans cells. *PLoS Pathog* 7:e1002100

Zhu T, Mo H, Wang N *et al.* (1993) Genotypic and phenotypic characterization of HIV-1 patients with primary infection. *Science* 261: 1179–81

Published online 8 September 2011

Nucleic Acids Research, 2012, Vol. 40, No. 1 ***345–359***
doi:10.1093/nar/gkr694

Biochemical, inhibition and inhibitor resistance studies of xenotropic murine leukemia virus-related virus reverse transcriptase

Tanyaradzwa P. Ndongwe[1], Adeyemi O. Adedeji[1], Eleftherios Michailidis[1], Yee Tsuey Ong[1], Atsuko Hachiya[1], Bruno Marchand[1], Emily M. Ryan[1], Devendra K. Rai[1], Karen A. Kirby[1], Angela S. Whatley[1], Donald H. Burke[1,2], Marc Johnson[1], Shilei Ding[3], Yi-Min Zheng[1], Shan-Lu Liu[1,3], Ei-Ichi Kodama[4], Krista A. Delviks-Frankenberry[5], Vinay K. Pathak[5], Hiroaki Mitsuya[6], Michael A. Parniak[7], Kamalendra Singh[1] and Stefan G. Sarafianos[1,2,*]

[1]Christopher Bond Life Sciences Center, Department of Molecular Microbiology & Immunology, University of Missouri, School of Medicine, Columbia, [2]Department of Biochemistry, University of Missouri, Columbia, MO 65211, USA, [3]Department of Microbiology and Immunology, McGill University, Montreal, QC, Canada, [4]Department of Internal Medicine, Division of Emerging Infectious Diseases, Tohoku University School of Medicine, Sendai, Japan, [5]HIV Drug Resistance Program, National Cancer Institute-Frederick, Frederick MD, [6]Department of Internal Medicine, Kumamoto University School of Medicine, Kumamoto Japan & Experimental Retrovirology Section, HIV/AIDS Malignancy Branch, NIH, Bethesda MD and [7]Department of Molecular Genetics & Biochemistry, University of Pittsburgh School of Medicine, Pittsburgh, PA, USA

Received June 3, 2011; Revised August 5, 2011; Accepted August 8, 2011

ABSTRACT

We report key mechanistic differences between the reverse transcriptases (RT) of human immunodeficiency virus type-1 (HIV-1) and of xenotropic murine leukemia virus-related virus (XMRV), a gammaretrovirus that can infect human cells. Steady and pre-steady state kinetics demonstrated that XMRV RT is significantly less efficient in DNA synthesis and in unblocking chain-terminated primers. Surface plasmon resonance experiments showed that the gammaretroviral enzyme has a remarkably higher dissociation rate (k_{off}) from DNA, which also results in lower processivity than HIV-1 RT. Transient kinetics of mismatch incorporation revealed that XMRV RT has higher fidelity than HIV-1 RT. We identified RNA aptamers that potently inhibit XMRV, but not HIV-1 RT. XMRV RT is highly susceptible to some nucleoside RT inhibitors, including Translocation Deficient RT inhibitors, but not to non-nucleoside RT inhibitors. We demonstrated that XMRV RT mutants K103R and Q190M, which are equivalent to HIV-1 mutants that are resistant to tenofovir (K65R) and AZT (Q151M), are also resistant to the respective drugs, suggesting that XMRV can acquire resistance to these compounds through the decreased incorporation mechanism reported in HIV-1.

INTRODUCTION

Xenotropic murine leukemia virus-related virus (XMRV) is a gammaretrovirus that was first identified in some prostate cancer tissues (1,2) While some subsequent reports confirmed the presence of XMRV in prostate cancer samples (3–6), several others found little or no evidence of the virus in patient samples (7–9). XMRV DNA was also reported in 67% of patients with chronic fatigue syndrome (CFS) (10), but several subsequent studies in Europe and the USA failed to identify XMRV DNA in CFS patients or healthy controls (11–15). Hence, the relevance of XMRV to human disease remains unclear (16) and have been challenged (17). Most recently, it has been reported that XMRV has been generated through recombination of two separate proviruses suggesting that the association of XMRV with human disease is due to contamination of human samples with virus originating from this recombination event (18). Nonetheless, as a retrovirus that can infect human cells, XMRV can be very helpful in advancing our understanding of the mechanisms of retroviral reverse transcription, inhibition and drug resistance.

*To whom correspondence should be addressed. Tel: +1 573 882 4338; Fax: +1 573 884 9676; Email: sarafianoss@missouri.edu

XMRV RT is similar to the Moloney murine leukemia virus (MoMLV) RT, which has been the subject of structural and biochemical studies (19–24). Most of the differences between these gammaretroviral enzymes are at the RNase H domain (Supplementary Figure S1). Comparisons of human immunodeficiency virus type-1 (HIV) RT with MoMLV RT have revealed structural and sequence differences (21). For example, HIV-1 RT is a heterodimer composed of two related subunits (25,26) [reviewed in (27,28)]. Its larger p66 subunit (~66 kDa) contains both the polymerase and RNase H domains; the smaller p51 subunit, (~51 kDa), is derived from the p66 subunit by proteolytic cleavage and its role is to provide structural support and optimize RT's biochemical functions (29). In contrast, structural studies have demonstrated that MoMLV RT is a monomer of about 74 kDa, although one study reported that it may form a homodimer during DNA synthesis (30). So far, there are no published biochemical or structural studies on XMRV RT. Hence, the present study on this enzyme and its comparison to related enzymes provides an excellent opportunity to advance our biochemical understanding of the mechanism of reverse transcription, its inhibition and drug resistance.

MATERIALS AND METHODS

Expression and purification of XMRV, HIV-1 and MoMLV RTs

The plasmid pBSK-XMRV containing the coding sequence of XMRV RT from the VP62 clone (GenBank: DQ399707.1) was chemically synthesized and optimized for bacterial expression by Epoch Biolabs Inc (Missouri City, Texas, USA). The 2013 bp XMRV RT sequence was amplified from pBSK-XMRVRT by PCR, using the forward and reverse primers 1 (all primer sequences are shown in Supplementary Table S1), resulting in NdeI and HindIII restriction sites. Drug resistant XMRV RT mutants Q190M and K103R (equivalent to HIV-1 Q151M RT and K65R) were generated by site-directed mutagenesis using forward and reverse primers 2 and 3. The digested amplicons were ligated into pET-28a (Novagen), resulting into a construct that expresses an N-terminal hexahistidine tag. pET-28a-MRT encoding full-length wild-type MoMLV RT was provided by Dr M. Modak (New Jersey Medical School, Newark NJ, USA).

Expression and purification of MoMLV and XMRV RTs were carried out similarly to our previously published protocols (23,24). Briefly, RTs were expressed in BL21-pLysS *Escherichia coli* (Invitrogen) grown at 37°C and induced with 150 μM IPTG at OD_{600} 0.8, followed by 16 h growth at 17°C. A cell pellet from a 3 l culture was incubated with 40 ml lysis buffer (50 mM Tris–HCl, pH 7.8, 500 mM NaCl, 1 mM PMSF, 0.1% NP-40, 1% sucrose and 2 mg/ml lysozyme), then sonicated and centrifuged at 15,000 *g* for 30 min. The supernatant was diluted 2-fold in Buffer A (50 mM Tri–HCl pH 7.8, 1 mM PMSF, 4% streptomycin sulfate and 10% sucrose), stirred on ice for 30 min and centrifuged. The supernatant was loaded on a Ni-NTA column and bound proteins were washed with 20 ml Buffer B (20 mM Tris–HCl pH 7.5, 500 mM NaCl) and 5 mM imidazole, followed by 20 ml Buffer B with 75 mM imidazole. RT was eluted in 2 ml fractions with 20 ml buffer B containing 300 mM imidazole. Fractions with RT were pooled and further purified by size exclusion chromatography (Superdex 75; GE Healthcare). RTs (>95% pure) were stored in 50 mM Tris–HCl pH 7.0, 100 mM NaCl, 1 mM DTT, 0.1% NP-40 and 30% glycerol in 10 μl aliquots at −20°C. Protein concentrations were determined by measuring UV_{280} (molar extinction coefficients of 106 and 103 $M^{-1} cm^{-1}$ for XMRV and MoMLV RT).

HIV-1 RT was cloned in a pETduo vector and purified as described previously (29,31,32). Oligonucleotide sequences (IDT-Coralville, IA, USA) of DNA/RNA substrates are shown in Supplementary Table S1. Nucleotides were purchased from Fermentas (Glen Burnie, MD, USA). They were treated with inorganic pyrophosphatase (Roche Diagnostics, Mannheim, Germany) as described previously (33) to remove PPi that might interfere with excision assays.

Steady state kinetics

Steady state parameters K_m and k_{cat} for dATP incorporation were determined using single nucleotide incorporation gel-based assays. XMRV RT and MoMLV RT reactions were carried out in 50 mM Tris–HCl pH 7.8, 60 mM KCl, 0.1 mM DTT, 0.01% NP-40 and 0.01% bovine serum albumin (BSA) (Reaction Buffer) with 6 mM $MgCl_2$ or 1.5 mM $MnCl_2$, 0.5 mM EDTA, 200 nM or 100 nM T_{d26}/5′-Cy3-P_{d18b}, 20 nM or 5 nM RT for XMRV and MoMLV RTs, respectively and varying concentrations of dNTP in a final volume of 10 μl. The reactions for HIV-1 RT were carried out in Reaction Buffer with 100 nM T_{d26}/5′-Cy3-P_{d18b}, 10 nM HIV-1 RT and 6 mM $MgCl_2$ in a 20 μl reaction. All the concentrations mentioned here and in subsequent assays reflect final concentration of reactants otherwise mentioned reactions were stopped after 15 min for XMRV, 4 min for MoMLV RT, and 2.5 min for HIV-1. The products were resolved on 15% polyacrylamide–7M urea gels. The gels were scanned with a Fuji Fla-5000 PhosphorImager (Stamford, CT, USA) and the bands were quantified using MultiGauge. Results were plotted using GraphPad Prism 4. K_m and k_{cat} were determined graphically using Michaelis–Menten equation.

Gel mobility shift assays

Formation of RT-DNA binary complex: 20 nM T_{d31}/5′-Cy3-P_{d18a} (Supplementary Table S1) was incubated for 10 minutes with increasing amounts of MoMLV or XMRV RT in 50 mM Tris–HCl pH 7.8, 0.01% BSA, 5 mM $MgCl_2$ and 10% (v/v) sucrose. The complexes were resolved on native 6% polyacrylamide 50 mM Tris–borate gel and visualized as described above.

Active site titration and determination of $K_{D.DNA}$

Active site concentrations and kinetic constants of DNA binding for XMRV, HIV-1 and MoMLV RTs were determined using pre-steady state experiments. Reactions

with XMRV and MoMLV RTs were carried out in the reaction buffers listed above. For XMRV RT 100 nM protein was pre-incubated with increasing concentrations of T_{d31}/5′-Cy3-P_{d18a}, followed by rapid mixing with a reaction mixture containing 5 mM $MgCl_2$ and 100 μM next incoming nucleotide (dATP). The reactions were quenched at various times (5 ms to 4 s) by adding EDTA to a final concentration of 50 mM. The amounts of 19-mer product were quantified and plotted against time. The data were fit to the following burst equation:

$$P = A(1 - e^{-k_{obs}t}) + k_{ss}t \quad (1)$$

where A is the amplitude of the burst phase that represents the RT–DNA complex at the start of the reaction, k_{obs} is the observed burst rate constant for dNTP incorporation, k_{ss} is the steady state rate constant and t is the reaction time. The rate constant of the linear phase (k_{cat}) was estimated by dividing the slope of the linear phase by the enzyme concentration. The active site concentration and T/P binding affinity ($K_{D.DNA}$) were determined by plotting the amplitude (A) against the concentration of T/P. Data were fit to the quadratic equation (Equation 2) using non-linear regression:

$$A = 0.5(K_D + [RT] + [DNA] - \sqrt{0.25(K_D + [RT] + [DNA])^2} - ([RT] + [DNA]) \quad (2)$$

where K_D is the dissociation constant for the RT–DNA complex, and [RT] is the concentration of active polymerase. HIV-1 RT's DNA binding affinity was determined as previously described (29).

Surface plasmon resonance assay

We used surface plasmon resonance (SPR) to measure the binding constants of XMRV and HIV-1 RTs to double-stranded DNA. Experiments were carried out using a Biacore T100 (GE Healthcare). To prepare the sensor chip surface we used the 5′-biotin-T_{d37}/P_{d25} oligonucleotide (Supplementary Table S1). One hundred and twenty RUs of this DNA duplex were bound in channel 2 of a streptavidin-coated sensor chip [Series S Sensor Chip SA (certified)] by flowing a solution of 0.1 μM DNA at a flow rate of 10 μl/min in a buffer containing 50 mM Tris pH 7.8, 50 mM NaCl. The binding constants were determined as follows: RT binding was observed by flowing solutions containing increasing concentrations of the enzyme (0.2, 0.5, 1, 2, 5, 10, 20, 50, 100 and 200 nM) in 50 mM Tris pH 7.8, 60 mM KCl, 1 mM DTT, 0.01% NP40 and 10 mM $MgCl_2$ in channels 1 (background) and 2 (test sample) at 30 μl/min. The trace obtained in channel 1 was subtracted from the trace in channel 2 to obtain the binding signal of RT. This signal was analyzed using the Biacore T100 Evaluation software to determine $K_{D.DNA}$, k_{on} and k_{off}.

Pre-steady state kinetics of dNTP incorporation

The optimal nucleotide incorporation rates (k_{pol}) were obtained by pre-steady state kinetics analysis using single nucleotide incorporation assays. A solution containing XMRV RT (150 nM final concentration) and T_{d31}/5′-Cy3-P_{d18a} (40 nM) was rapidly mixed with a solution of $MgCl_2$ (5 mM) and varying dATP (5–200 μM) for 0.1 to 6 s before quenching with EDTA (50 mM) (all concentrations in parentheses are final, unless otherwise stated). Products were resolved and quantified as described above. Burst phase incorporation rates and substrate affinities were obtained from fitting the data to Equation 1. Turnover rates (k_{pol}), dNTP binding to the RT-DNA complex ($K_{d.dATP}$), and observed burst rates (k_{obs}) were fit to the hyperbolic equation:

$$k_{obs} = (k_{pol}[dNTP])/(K_{d.dNTP} + [dNTP]) \quad (3)$$

HIV-1 RT's DNA binding affinity was determined as previously described (29).

Fidelity of DNA synthesis

The fidelity (error-proneness) of XMRV RT was determined and compared with that of MoMLV RT and HIV-1 RT by primer extension assays using 10 nM heteropolymeric T_{d100}/5′-Cy3-P_{d18a}. Reactions (10 μl) were carried out in Reaction Buffer containing all four dNTPs (100 μM each) or only three dNTPs (missing either dATP, dGTP or dTTP) at 100 μM each. Incubations of the XMRV and MoMLV (50 nM) reactions were at 37°C for 45 min and 30 min for HIV-1 RT (20 nM). Reactions were initiated by adding dNTPs, stopped with equal volume of formamide-bromophenol blue, and an aliquot was run on a 16% polyacrylamide–7M urea gel.

Kinetics of mismatch incorporation

For these experiments, instead of including the next correct nucleotide (dATP) in the polymerase reactions, we used dTTP as the mismatched incoming nucleotide. Hence, 50 nM XMRV RT was pre-incubated with 35 nM T_{d31}/5′-Cy3-P_{d18a} in reaction mixture. Reactions were initiated by adding dTTP (5–750 μM) and 5 mM $MgCl_2$, followed by incubation (37°C) for 5 min, due to the decreased mismatch incorporation rate of XMRV. For MoMLV RT, 30 nM RT and 20 nM DNA used and the reactions were carried out for 2.5 minutes. For HIV-1, 30 nM RT, 20 nM DNA and 0–200 μM nucleotide were used and the reactions were carried out for 2.5 min. The amount of extended primer was quantified and plotted against the concentration of dTTP. The data were used to derive the $K_{d.dNTP}$ of incorrect nucleotide binding, the rate k_{pol} (using Equations 1 and 3) and the efficiency of the misincorporation reaction ($k_{pol}/K_{d.dTTP}$).

Determination of *in vivo* fidelity

ANGIE P cells, which contain a retroviral vector (GA-1) that encodes a bacterial β-galactosidase gene (*lacZ*) and a neomycin phosphotransferase gene, were plated (5×10^6 cells/100 mm dish) and after 24 h were transfected using the calcium phosphate precipitation method with a plasmid expressing either XMRV or amphotropic MLV (AM-MLV) (three independent transfections per vector). After 48 h, the culture medium with XMRV or (AM-MLV) was harvested, serially diluted and used to infect

D17 target cells (2×10^5 cells/60 mm dish) in the presence of polybrene. The infected D17 cells were selected for resistance to G418 (400 μg/ml) in the presence of 1 μM AZT to suppress reinfection, and characterized by staining with 5-bromo-4-chloro-3-indoyl-β-D-galacto-pyranoside (X-Gal) ~2 weeks after G418 selection. The frequencies of inactivating mutations in *lacZ* quantified as described before (blue versus white colonies) (34).

Processivity of DNA synthesis—trap assay

Processivity reactions were carried out in Reaction Buffer containing 20 nM T_{d100}/P_{d18}, 100 μM of each dNTP, 30 nM HIV-1 RT, 50 nM MoMLV RT or 100 nM XMRV RT and 1 μg/μl unlabeled calf thymus DNA trap in 50 μL. Enzymes were pre-incubated with T_{d100}/P_{d18} for 1 min before adding dNTPs (100 μM each) together with the calf thymus DNA trap. Reactions were incubated at 37°C, and 10 μl aliquots were taken out at 3, 7.5 and 15 min for HIV-1 RT or at 7.5, 15 and 30 min for XMRV RT and MoMLV RT, and mixed with equal volume of loading dye. The effectiveness of the trap was determined by pre-incubating the enzyme with the trap before adding T_{d100}/P_{d18}. Control DNA synthesis was measured in absence of trap under the same conditions. Reaction products were resolved as above.

Single turnover processivity assays

Thirty nanomolar $T_{d31}/5'$-Cy3-P_{d18a} was pre-incubated for 10 min with 100 nM XMRV or 50 nM MoMLV RT in Reaction Buffer, then rapidly mixed with 100 μM dNTPs, 5 mM $MgCl_2$ for varying times (0.1–45 s) before quenching with EDTA (50 mM final). Single turnover processivity of HIV-1 RT was assayed with 40 nM enzyme, 20 nM DNA and 50 μM of each nucleotide were used. The reaction products were resolved and quantified as described above. The data were fit to a one-phase exponential decay equation for the elongation of the 18-mer primer. The rates of appearance and extension of products from subsequent nucleotide incorporations (19- and 27-mer) were obtained by fitting the intensities of corresponding bands to double exponential (Equation 4):

$$P = A(1 - e^{-k_1 t}) + (e^{-k_2 t}) + C \quad (4)$$

where A is the amplitude, P is the amount of 19-mer, 20-mer or higher length products, k_1 is the rate of product generation, k_2 the rate of subsequent elongation and C a constant (29,35).

Assays for reverse transcriptase inhibition

DNA synthesis by 50 nM XMRV RT or MoMLV RT was carried out in Reaction Buffer using 20 nM $T_{d100}/5'$-Cy3-P_{d18a}, 2.5 μM dNTP, 5 mM $MgCl_2$ and varying amounts of NRTI (0–100 μM). Reactions were quenched with 95% formamide after 1 h incubation at 37°C (38). In experiments with aptamers 10 nM XMRV RT, 20 nM $T_{d31}/5'$-Cy3-P_{d18a} and 50 μM dNTPs were used in the presence of varying amounts of aptamer for 30 min (0–500 nM for m.1.3; 0–25 nM for m.1.4 and m.1.1FL). The inhibition of DNA polymerization was monitored by resolving the products on 15% polyacrylamide–7 M urea gels and visualized as described above. Bands corresponding to full extension products were quantified using MultiGauge Software and IC_{50}s were obtained from dose–response curves using GraphPad Prism.

PPi- and ATP-dependent excision and rescue of $T/P_{AZT\text{-}MP}$ or $T/P_{EFdA\text{-}MP}$

The ability of enzymes to use PPi or ATP to unblock template-primers that had AZT-MP ($T/P_{AZT\text{-}MP}$) or EFdA-MP ($T/P_{EFdA\text{-}MP}$) at their 3′ primer ends was measured as follows: 20 nM of $T/P_{AZT\text{-}MP}$ or $T/P_{EFdA\text{-}MP}$ were prepared as described before (32). They were incubated at 37°C with either 60 nM HIV-1 RT or 200 nM XMRV RT in the presence of 0.15 mM PPi or 3.5 mM ATP for PPi- or ATP-dependent rescue reactions, respectively. Reactions were initiated by the addition of $MgCl_2$ (6 mM). Aliquots were removed at different times (0–90 min) and analyzed as above. Rescue assays were performed in the presence of 100 μM dATP to prevent EFdA-MP reincorporation, 0.5 μM dTTP, 10 μM ddGTP and 10 mM $MgCl_2$.

Molecular modeling

The sequence of XMRV RT from the VP62 clone was aligned with that of MoMLV RT (PDB: 1RW3) (21,22) using ClustalW. To generate the homology model of XMRV RT, we used the Prime protocol of the Schrödinger software suite (Schrödinger Inc. NY). The resulting molecular model was further energy minimized by OPLS2005 force field using the Impact option of Schrödinger. The final model was validated with PROCHECK v.3.5.4.

RESULTS

Comparison of RT sequences

The XMRV and MoMLV enzymes are closely related (~95% sequence identity) with most of the differences between them being in the RNase H domain (Supplementary Figure S1). While XMRV and MoMLV differ significantly from HIV-1 RT, the known polymerase motifs (A–F) are well conserved in all three enzymes (Supplementary Figure S1). Specifically, the active site aspartates in Motifs A and C (Figure 9) (D150, D224, D225 in XMRV RT; D150, D224, D225 in MoMLV RT; D110, D185, D186 in HIV-1 RT) are conserved in all three RTs. Also, the three enzymes are similar in Motif B, which is involved in dNTP binding and multidrug resistance (AZT and dideoxy-nucleoside drugs) through the decreased incorporation mechanism (27,39–41). Specifically, all three enzymes have a glutamine at the start of this motif (Q151 in HIV-1 RT, Q190 in XMRV RT and Q190 in MoMLV RT). Motif D includes HIV-1 RT residues L210 and T215, which when mutated they enhance excision of AZT from the AZT-terminated primer terminus. This motif is mostly different in XMRV and MoMLV RTs, where the corresponding residues are N226 and A231 (Supplementary Figure S1). K219 of HIV-1 RT Motif D is proximal to

the dNTP-binding pocket and is also conserved in the other enzymes (K235). The DNA primer grip (Motif E) (36,42) in HIV-1 RT ($M_{230}G_{231}Y_{232}$) is slightly different in the gammaretroviral enzymes ($L_{245}G_{246}Y_{247}$). Motif F at the fingers subdomain of all enzymes has two conserved lysines that bind the triphosphate of the dNTP (K65 and K72 in HIV-1 RT; K103 and K110 in XMRV and MoMLV RTs).

Several HIV-1 residues involved in NRTI resistance have the resistance mutations in XMRV and MoMLV RTs (Table 1). Hence, XMRV and MoMLV RTs have a Val as the X residue (codon 223) of the conserved YXDD sequence of Motif C. An M184V mutation at this position in HIV-1 RT causes strong, steric hindrance-based, resistance to 3TC and FTC (43–45), and to a lesser extent to ddI, ABC [reviewed in (46)], and translocation defective RT inhibitors (TDRTIs) (43) (Table 1). Similarly, the M41L mutation, which causes excision-based AZT resistance in HIV is already present in XMRV and MoMLV RT (L81, Table 1). The gammaretroviral enzymes differ from HIV-1 RT in several other HIV drug resistance sites (HIV residues 62, 67, 69, 70, 75, 77, 115, 210, 215) (Table 1). Finally, there are also differences in residues that are essential for NNRTI binding in HIV-1 RT: W229 changes to Y268 in XMRV RT, Y181 to L220, Y188 to L227 and G190 to A229 (Table 1) (27,28,47–49).

Preparation of MoMLV and XMRV RTs

The sequence coding for full-length XMRV RT from the VP-62 clone (NCBI RefSeq: NC_007815) (1) was optimized for expression in bacteria, synthesized by Epoch Biolabs and cloned as described in 'Materials and Methods' section. Both XMRV RT and MoMLV RT were tagged with a hexahistidine sequence at the N-terminus and expressed with a yield of ~2 mg/l of culture. Purified enzymes (>95% pure, Supplementary Figure S2) were stored at −20°C. The presence of NP-40 or glycerol was critical for enzyme stability.

Steady state kinetics of nucleotide incorporation

Initial polymerase activity assays using $T_{d31}/5'$-Cy3-P_{d18a} displayed overall slower polymerase activity of XMRV RT compared to HIV-1 and MoMLV RTs. This observation led us to investigate the steady state nucleotide incorporation properties of XMRV RT using single nucleotide incorporation assays. The estimated values for k_{cat} (19.9 min^{-1} for HIV-1 RT (32), 3.3 min^{-1} for MoMLV RT, 0.6 min^{-1} for XMRV RT) and $K_{m.dNTP}$ (0.07 μM for HIV-1 RT (32), 3.3 μM for MoMLV RT, 3.0 μM for XMRV RT) show that XMRV RT has a drastically reduced efficacy ($k_{cat}/K_{m.dNTP}$) at nucleotide incorporation, compared to both MoMLV and HIV-1 RTs.

DNA binding affinity

To assess if the efficiency of XMRV RT was also affected by a lower DNA binding affinity we measured the DNA binding affinity of the enzymes using three methods: gel-mobility shift assays, pre-steady state kinetics and SPR. Gel-mobility shift assays showed that the $K_{D.DNA}$ for XMRV RT was marginally higher than that for HIV-1 RT and MoMLV RT (data not shown) (50) suggesting weaker binding to DNA.

DNA binding affinity using pre-steady state kinetics

Pre-steady state kinetics allows estimation of the fraction of active polymerase sites as well as the $K_{D.DNA}$ value for the enzyme. The amplitudes of DNA extensions using XMRV RT and/or MoMLV RT at varying DNA concentrations were plotted against the DNA concentration and

Table 1. HIV-1 RT drug resistance mutations with wild-type XMRV RT and MoMLV RT residues

	HIV-1 residue numbers	HIV-1 RT wt	HIV-1 resistance mutations					XMRV RT wt	MoMLV RT wt
			3TC	ABC	TDF	D4T	EFdA		
Thymidine analog mutations (TAMs)	184	M	V	V	–	–	V	V223	V223
	41	M	–	L	L	L	–	L81	L81
	67	D	–	N	N	N	–	G105	G105
	210	L	–	W	W	W	–	N226	N226
	215	T	–	FY	FY	FY	–	A231	A231
	219	K	–			QE	–	K235	K235
Non-thymidine analog regimen mutations	65	K	RN	RN	RN	RN	–	K103	K103
	70	K	EG	EG	EG	–	–	D108	D108
	74	L	–	VI	–	–	–	V112	V112
	75	V	–	TM	M	TM	–	Q113	Q113
	115	Y	–	F	F		–	F155	F155
	69	T	Ins	Ins	Ins	Ins	–	N107	N107
Multi-NRTI resistance mutations	151	Q	M	M	M	M	–	Q190	Q190
	62	A	V	V	V	V	–	P104	P104
	75	V	–	I	–	I	–	Q113	Q113
	77	F	–	L	–	L	–	L115	L115
	116	F	–	Y	–	Y	–	F156	F156
TDRTI Mutations	184	M	V	V	–	–	V	V223	V223
	165	T	–	–	–	–	R	H204	H204

The HIV-1 RT data are based on data from the Stanford HIV Database (85).
wt = wild-type.

the data were fit to the quadratic equation (Equation 2), yielding a $K_{D.DNA}$ of 33 nM for XMRV RT, 19 nM for MoMLV RT (Table 2) and 12.5 nM for HIV-1 RT (32). These values did not change significantly when tested with DNA of different lengths (data not shown). Hence, the transient kinetic experiments confirmed the findings of the gel-mobility shift assays showing XMRV RT to have lower DNA binding affinity than HIV-1 RT.

Binding kinetics of XMRV and HIV-1 RT to double-stranded DNA

Measurements of $K_{D.DNA}$ using gel-mobility shift assays and pre-steady state kinetic methods do not offer insights regarding the kinetics of binding and release of nucleic acid from the viral polymerases. Hence, we used SPR to measure directly DNA binding and the DNA dissociation components of the $K_{D.DNA}$. We attached on the SPR chip a nucleic acid biotinylated at the 5′ template end and immobilized it on a streptavidin sensor chip. Various concentrations of either XMRV or HIV-1 RT were flowed over the chip to measure the association (k_{on}) and dissociation (k_{off}) rates of the enzymes in real time (Figure 1). HIV-1 RT had considerably slower dissociation rates than XMRV RT, and longer dissociation phases were needed to obtain reliable values.

Several methods were tested to best fit our data. The 'heterogeneous ligand' method gave the best fit for both XMRV and HIV-1 RT. In this model the x^2 values for DNA binding to XMRV and HIV-1 RT were 9.3 RU^2 and 48.1 RU^2, respectively, compared to 15.1 RU^2 and 152 RU^2 when we tried fitting the data in a 'homogeneous ligand' model. The former model assumes that RT binds DNA in two different modes and provides two association (k_{on}) and two dissociation constants (k_{off}).

Our data show that XMRV RT has a slightly faster rate of association (k_{on}) than HIV-1 RT. We measured two k_{on} values of $7.3 \times 10^6 M^{-1}s^{-1}$ and $8.2 \times 10^4 M^{-1}s^{-1}$ for XMRV RT versus $7.6 \times 10^5 M^{-1}s^{-1}$ and $1.2 \times 10^6 M^{-1}s^{-1}$ for HIV-1 RT. Interestingly, the dissociation rate of XMRV RT was significantly faster than that of HIV-1 RT ($0.28\,s^{-1}$ and $0.0045\,s^{-1}$ for XMRV RT and 7.8×10^{-4} $s^{-1}$and $0.0076\,s^{-1}$ for HIV-1 RT) (Table 3). This difference in dissociation rate resulted in a $K_{D.DNA}$ at least 1 order of magnitude higher for XMRV RT compared to HIV-1 RT (38 and 54 nM versus 1.0 and 6.1 nM for XMRV and HIV-1 RT, respectively) (Table 3).

Table 2. Kinetic parameters of DNA binding and synthesis by HIV-1 and XMRV RTs

Nucleotide affinity and incorporation	HIV-1 RT[a]	MoMLV RT	XMRV RT
$K_{d.dNTP}$ (μM)	1.3 ± 0.4	25 ± 5.3	26.6 ± 6.5
k_{pol} (s^{-1})	24.4 ± 0.9	14.1 ± 0.8	8.9 ± 0.6
$k_{pol}/K_{d.dNTP}$ ($s^{-1}\cdot\mu M^{-1}$)	18.8	0.56	0.33
DNA binding affinity:			
$K_{D.DNA}$ (nM)	12.5	19.0	32.5

[a]HIV-1 RT data published previously (29).

Nucleotide binding affinity and optimal incorporation efficiency

A transient-state kinetics approach was used to estimate the dNTP binding affinity ($K_{d.dNTP}$) and maximum nucleotide incorporation rate (k_{pol}) (55). The rates at varying concentrations of next incoming nucleotide (dATP) were determined by plotting the amount of extended primer as a function of time. The rates were then plotted against dATP concentration. The data were fit to a hyperbola (Equation 3). The $K_{d.dNTP}$ for XMRV RT is 26.6 μM and the k_{pol} is $8.9\,s^{-1}$ (Figure 2) (Table 2). Under similar conditions the $K_{d.dNTP}$ and k_{pol} were 1.3 μM and $24.4\,s^{-1}$ for HIV-1 RT (29) and 25 μM and $14.1\,s^{-1}$ for MoMLV RT.

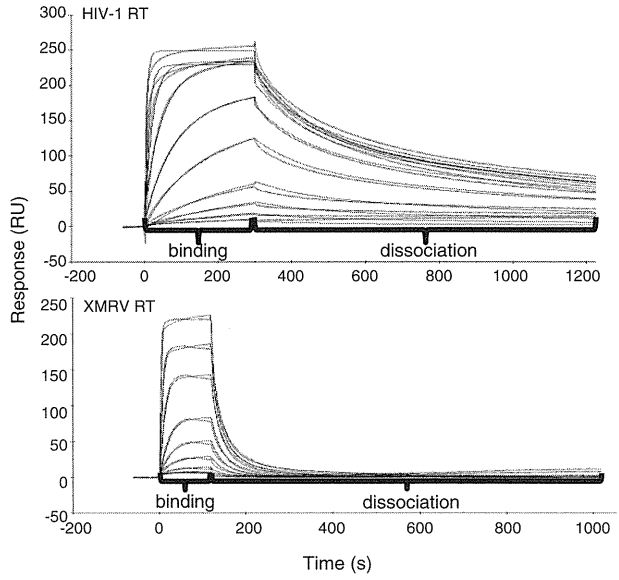

Figure 1. Assessment of $K_{D.DNA}$, k_{on} and k_{off} using surface plasmon resonance. SPR was used to measure the binding affinity of RTs to a nucleic acid substrate. Increasing concentrations of each RT (0.2, 0.5, 1, 2, 5, 10, 20, 50, 100 and 200 nM) were injected over a streptavidin chip with biotinylated double-stranded DNA immobilized on its surface as described in 'Materials and Methods' section. The experimental trace (red) shown is the result of a subtraction of the data obtained from the channel containing the immobilized nucleic acid minus the signal obtained from an empty channel. The black curve represents the fitted data according to the 'heterogeneous ligand' model that assumes two different binding modes for RT on the nucleic acid.

Table 3. DNA binding constants for HIV-1 and XMRV RTs from surface plasmon resonance

	HIV-1 RT	XMRV RT
k_{on} ($M^{-1}.s^{-1}$)	7.6×10^5	7.3×10^6
k_{off} (s^{-1})	7.8×10^{-4}	2.8×10^{-1}
$K_{D.DNA1}$ (nM)	1	38 (38-fold)[a]
k_{on} ($M^{-1}.s^{-1}$)	1.2×10^6	8.2×10^4
k_{off} (s^{-1})	7.6×10^{-3}	4.5×10^{-3}
$K_{D.DNA2}$ (nM)	6.1	54 (9-fold)[a]

[a]Increase in $K_{D.DNA}$ (decrease in affinity) with respect to HIV-1 RT. ($K_{D1\text{-}XMRV\ RT}/K_{D1HIV\text{-}1\text{-}RT}$ and $K_{D2\text{-}XMRV\ RT}/K_{D2HIV\text{-}1\text{-}RT}$).

Fidelity of nucleotide incorporation

To assess whether XMRV RT displays high nucleotide incorporation fidelity we monitored the incorporation of three dNTPs by XMRV RT and compared with HIV-1 RT (52). The results of fidelity assay are shown in Figure 3. The lanes marked '4dNTPs' for all enzymes represent the DNA synthesis using a T_{d100}/5′-Cy3-P_{d18a} template-primer in the presence of all four dNTPs. The subsequent lanes, marked '-dNTP', correspond to the synthesis of DNA in the absence of that specific deoxynucleotide triphosphate. The comparison of the DNA synthesis in the absence of one nucleotide by HIV-1 RT, MoMLV RT and XMRV RT shows that HIV-1 and MoMLV RTs were able to misincorporate and extend the primer beyond the missing nucleotide more efficiently than XMRV RT, suggesting that the latter is a less error prone DNA polymerase. It should be noted that the higher fidelity of XMRV is not the result of measuring a smaller number of errors because of the decreased replication rate, as the assay conditions were optimized to allow production of the same amount of full length product in the presence of all four dNTPs for and MoMLV RTs. To further investigate the fidelity of DNA synthesis by XMRV RT, the kinetics of mismatch nucleotide incorporation were carried out in a quantitative manner by monitoring the incorporation of single mismatched nucleotide under pre-steady state conditions. The estimated $K_{D.dTTP}$ (mismatch) and k_{pol} values show that XMRV RT has a lower affinity for a mismatched nucleotide but comparable turnover number than MoMLV RT, suggesting that the observed higher fidelity over MoMLV RT is due to differences during the nucleotide-binding step (Table 4). However, compared to HIV-1 RT, XMRV RT has decreased both affinity and incorporation rate, suggesting that its higher fidelity is the result of both decreased binding of mismatched nucleotides and slow rate of incorporation.

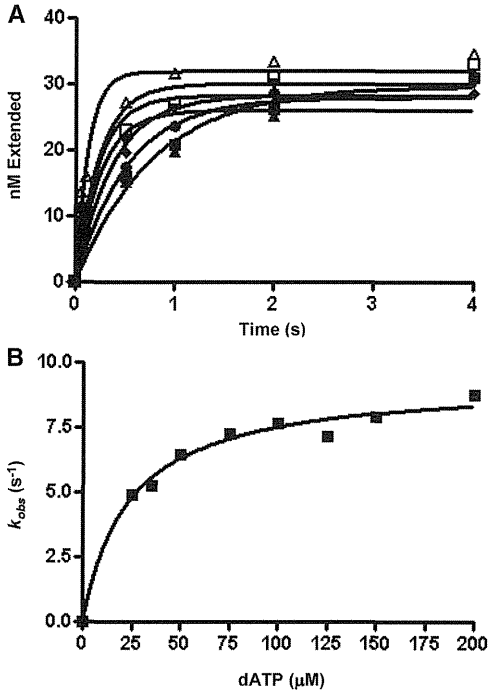

Figure 2. Pre-steady state kinetics of nucleotide incorporation by XMRV RT. 150 nM XMRV RT was pre-incubated with 40 nM T_{d31}/5′-Cy3-P_{d18a} rapidly mixed with a solution containing $MgCl_2$ (5 mM) and varying concentrations of dATP: 25 μM (filled square), 35 μM (filled triangle), 50 μM (filled inverted triangle), 75 μM (filled rhombus), 100 μM (filled circle), 125 μM (open square) and 150 μM (open triangle); and incubated for 0.1 to 6 s before being quenched with EDTA. The DNA product for each dATP concentration was fit to the burst equation (**A**). The burst amplitudes generated for each dATP concentration were then fit to a hyperbola equation (**B**) yielding the optimal rates of dNTP incorporation; k_{pol} ($8.9\,s^{-1}$) and dNTP binding to the RT-DNA complex; $K_{d.dATP}$ (26.6 μM).

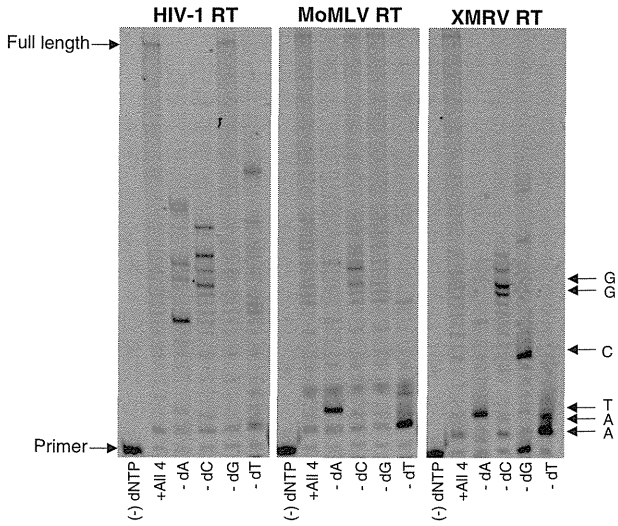

Figure 3. Comparison of *in vitro* fidelity of HIV-1, MoMLV and XMRV RTs. Extension of 10 nM T_{d100}/5′-Cy3-P_{d18a} by HIV-1 RT, MoMLV RT or XMRV RT (20, 50 and 50 nM, respectively) in the presence of 150 μM each of three out of four nucleotides (the missing nucleotide is marked at the bottom of each lane). Reactions were run for 30 min for HIV-1 RT and 45 min for XMRV RT and MoMLV RT. For each enzyme the first lane in each set shows the position of unextended primer, the second lane shows full extension in the presence of all four dNTPs, and each consecutive lane shows extension in the presence of three dNTPs. The arrows on the right mark the expected pauses based on the indicated composition of the template strand.

Table 4. Kinetics of mismatch incorporation for HIV-1, MoMLV and XMRV RTs

Enzyme	HIV-1 RT	MoMLV RT	XMRV RT
$K_{d.dNTP}$ (μM)	9 ± 0.3	38.9 ± 11.6	256 ± 72
k_{pol} (s^{-1})	6.81 ± 1.2	0.16 ± 0.01	0.15 ± 0.018
$k_{pol}/K_{d.dNTP}$ (s^{-1} • μM)	0.756	0.0041	0.00058
Fidelity[a]	0.04	0.007	0.002

[a]Fidelity is the ratio of the incorporation efficiency ($k_{pol}/K_{d.dNTP}$) of the mismatched nucleotide (dTTP) over that of the correct (dATP) ([k_{pol}/K_d]dTTP/[k_{pol}/K_d]dATP).

Intracellular fidelity by measuring LacZ mutation frequency

The ANGIE P cells used for this assay are a D17-based encapsidating cell line and contain an MLV-based retroviral vector (GA-1), which encodes a bacterial β-galactosidase gene (*lacZ*) and a neomycin phosphotransferase gene (*neo*). Replication fidelity is a measure of the frequency of *lacZ* inactivation and was determined by measuring *lacZ* non-expressing white colonies. The results show that the number of white colonies was not statistically different in the case of XMRV as compared to AM-MLV, suggesting that under these conditions the fidelity of XMRV is not significantly different than that of AM-MLV (Figure 4).

Processivity of DNA synthesis

Processivity is the probability of translocation of a polymerase along a template and predicts the number of cycles of nucleotide incorporation during one productive enzyme–DNA binding event. We assessed XMRV RT's processivity of DNA synthesis in comparison to HIV and MoMLV RTs using both a gel-based trap assay and a quantitative pre-steady state assay. In the gel-based assay, the enzymes were pre-incubated with template-primer, then the reaction was initiated by the addition of all four nucleotides together with calf thymus DNA, which was used as a trap to bind free enzyme dissociated from the substrate during the course of the reaction (38). The length of the DNA product is an inverse measure of termination probability, as previously described. As a control, we used lanes where no trap was present; establishing that the same amount of total polymerase activity (processive and non-processive) is provided in all cases. The results indicate that XMRV RT is less processive than HIV-1 and MoMLV RTs with shorter DNA product after 30 min of reaction in the presence of trap (Figure 5).

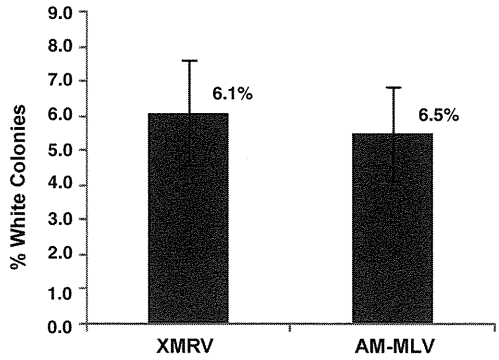

Figure 4. Comparison of *in vivo* fidelity of XMRV with amphotropic MLV. The ANGIE P cells used for this assay contain a retroviral vector (GA-1), which encodes a bacterial β-galactosidase gene (*lacZ*) and a neomycin phosphotransferase gene. Replication fidelity is measured by the frequency of *lacZ* inactivation resulting in an increase in white colonies. The fidelity differences between the two viruses are not statistically significant (error bars represent standard error from three independent experiments).

To measure processivity quantitatively we applied a single turnover processivity assay developed by Patel *et al.* (35) (Figure 6). In this assay, the rates of consecutive nucleotide incorporations under single turnover conditions are monitored. The rate of elongation incorporation (k_1) and the rate of processive DNA synthesis (k_2) (Equation 4) were calculated at several template positions for each enzyme. The ratio of the rate of processive DNA synthesis to the rate of nucleotide incorporation (k_2/k_1) is referred to as the processivity index (35). The absolute values of these constants for HIV-1 RT, XMRV and MoMLV RT and their ratios are collected in Table 5. XMRV RT is clearly the least processive for each extension product. The difference in processivity varies significantly depending on sequence or sequence context (decrease in processivity from 3-fold up to 10-fold). While the current data do not allow generalization of rules for pausing at specific sites, this clearly shows consistently that XMRV is not as efficient as MoMLV RT in polymerizing processively through 'difficult spots'.

Susceptibility of XMRV RT to NRTIs, TDRTIs and NNRTIs

Previous studies have shown that XMRV is inhibited by some antivirals (53–56). However, the susceptibility of XMRV RT has not been tested against a wide variety of

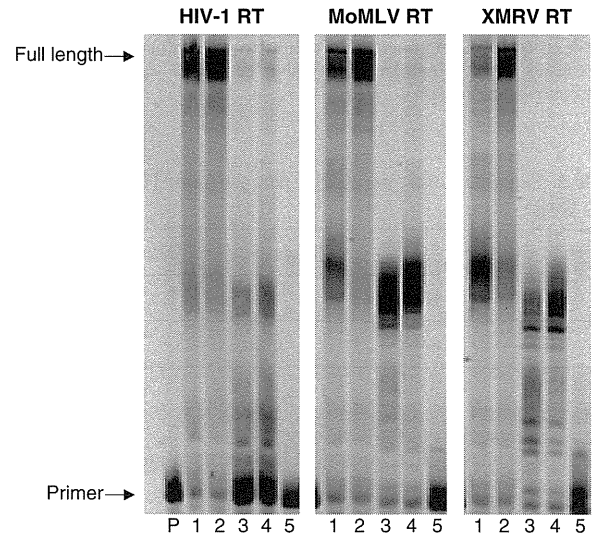

Figure 5. Processivity (trap assay) of HIV-RT, MoMLV RT and XMRV RT. DNA synthesis was monitored in the presence of calf thymus DNA as an enzyme trap. Each enzyme (30 nM HIV RT, 100 nM MoMLV RT or 100 nM XMRV RT) was pre-incubated with 40 nM T_{d100}/Cy3-P_{d18a}. Lanes 1 and 2 of each set show unlimited DNA synthesis in the absence of trap for 5 and 10 min for HIV-1 RT and 10 and 40 min for XMRV RT and MoMLV RT. In Lanes 3 and 4 the reaction is initiated by the addition of dNTPs (100 μM each) together with the calf thymus DNA trap (0.5 μg/μl) such that the products generated represent a single processive synthesis event for the respective time points for each enzyme. Lane 5 shows the effectiveness of the trap determined by incubating the calf thymus DNA with the enzyme before addition of labeled template-primer. Processive primer extension by HIV-1 RT and MoMLV RT in Lanes 4–6 of the left and middle panel is higher than by XMRV RT in Lanes 4–6 of the right panel.

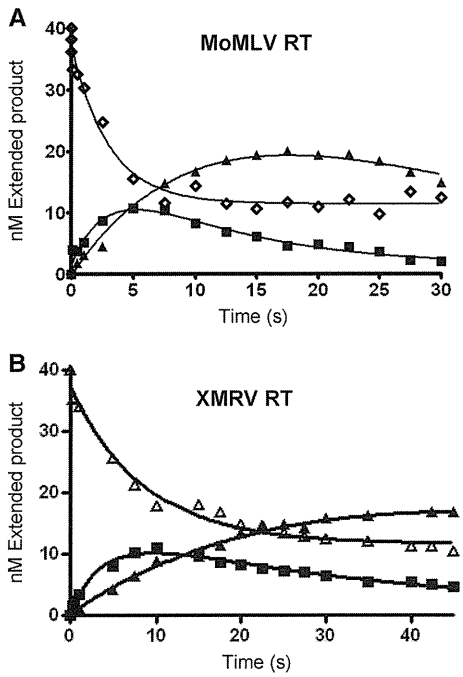

Figure 6. Single-turnover processivity assays. 30 nM T_{d31}/Cy3-P_{d18a} was combined with 100 nM XMRV RT or 50 nM MoMLV RT in RT buffer before rapidly mixing with all four dNTPs (100 μM each) and 5 mM $MgCl_2$ for varying incubation times (0.05–45 s) and quenching with EDTA. Extension of the 18-mer primer (open rhombus) ((open triangle) for XMRV RT) into 19-mer (filled square) and 22-mer (filled square), by MoMLV RT (**A**) and XMRV RT (**B**) was fit to a double exponential equation to determine rates of product appearance, and subsequent processive extension of those products (rates shown in Table 5).

Table 5. Single turnover processivity parameters of HIV-1, MoMLV and XMRV RTs

Template site	Processivity index (k_2/k_1)		
	HIV-1 RT	MoMLV RT	XMRV RT
1	6.98	0.31	0.12

1
3′-CAT TGA CAA GCT CGT GGT TAC GAT CGA TAC C
5′-Cy3-GTA ACT GTT CGA GCA CCT
The template site position monitored is underlined and labeled.

nucleoside RT inhibitors (NRTIs) that block replication by chain-terminating the primer, or by preventing translocation after their incorporation into the nascent DNA chain (TDRTIs) (32,57,58). In addition, the susceptibility of XMRV RT to non-nucleoside RT inhibitors (NNRTIs) or RNA aptamers that can be selected to block reverse transcriptases (59–63) has not been established.

Hence, we performed gel-based primer extension assays in the presence of various inhibitors. As shown in Table 6, most of the HIV-1 RT inhibitors also block XMRV RT with significantly varying IC_{50}s. The most potent inhibitors tested were ENdA (4′-ethynyl-2-amino-2′-deoxyadenosine) followed by EFdA. EFdA was also potent at

Table 6. Inhibition of XMRV and MoMLV RTs

Compound	IC_{50} (μM)	
	XMRV RT	MoMLV RT
Adefovir-DP	0.92	1.02
Tenofovir-DP	6.4	1.51
D4T-TP	0.77	2.37
3TC-TP	21	10
EFdA-TP	0.43	0.29
ENdA-TP	0.14	0.18

D4T, stavudine or 2′,3′-dehydro-2′,3′-deoxythymidine; 3TC, lamivudine; EFdA, 4′-ethynyl-2-fluoro-2′-deoxyadenosine; ENdA, 4′-ethynyl-2-amino-2′-deoxyadenosine.

inhibiting wild-type XMRV replication in cell culture with an EC_{50} of 40 nM from three independent experiments (standard error was 10 nM).

Unlike HIV-1 RT, XMRV RT and MoMLV RT lack the two tyrosine residues (Y181 andY188 in HIV-1 RT) (Supplementary Figure S1) that are known to contribute to NNRTI binding. Hence, the gammaretroviral enzymes were not inhibited by the NNRTIs tested (TMC-125 and efavirenz) (Supplementary Figure S3).

Susceptibility of XMRV RT to RNA aptamers

We also tested XMRV RT's susceptibility to three independent RNA aptamers that had been previously selected against MoMLV RT (60). The aptamers inhibited XMRV RT to varying extents with IC_{50}s ranging from 2 to 52 nM (Figure 7). Most notable was the m.1.1FL aptamer which gave IC_{50}s of 2 and 4 nM for XMRV RT (Figure 7) and MoMLV RT respectively, without inhibiting HIV-1 RT (data not shown). These inhibition assays utilized truncated forms of aptamers m.1.3 and m.1.4 lacking the original primer-binding segments of the aptamers, demonstrating that these 5′ and 3′ segments are not required.

PPi-mediated excision activity of XMRV RT

A key mechanism of NRTI resistance in HIV-1 RT is based on inhibitor excision from the primer end, using a pyrophospholytic reaction (64,65). The pyrophosphate donor *in vivo* is likely to be ATP, although PPi can efficiently unblock NRTI-terminated primers. This excision activity is present in wild-type HIV-1 RT, and is enhanced in the presence of AZT-resistance mutations. We measured the ability of wild-type XMRV to unblock primers terminated with AZT or EFdA in the presence of PPi. We found that unlike HIV-1 RT that excised AZT-MP efficiently under these conditions, XMRV RT had considerably lower excision activity (Figure 8). Similar excision experiments where ATP was used instead of PPi showed that XMRV is very inefficient in ATP-based excision as compared to HIV-1 RT (data not shown).

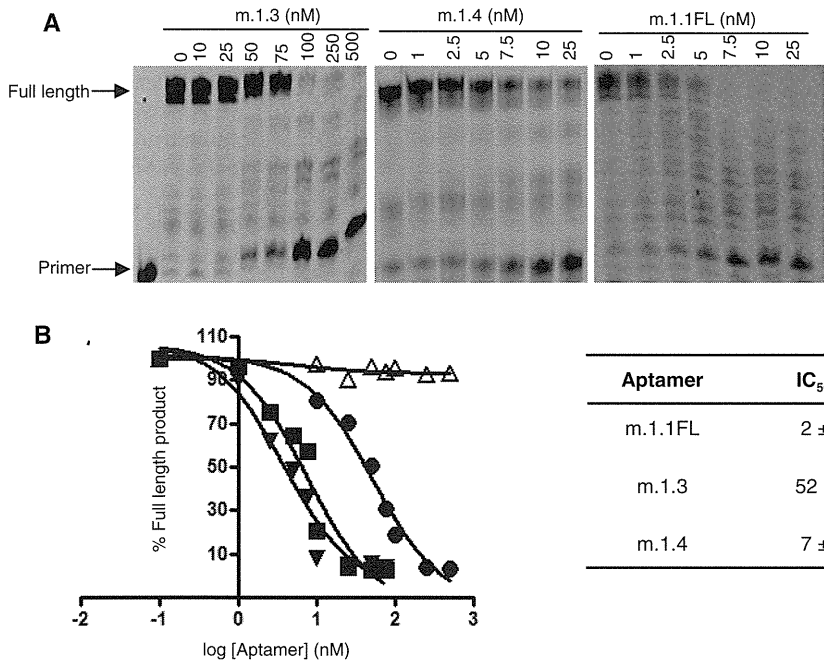

Aptamer	IC_{50} (nM)
m.1.1FL	2 ± 0.15
m.1.3	52 ± 0.27
m.1.4	7 ± 0.16

Figure 7. Inhibition of XMRV RT by RNA aptamers. 10 nM XMRV RT was incubated with increasing amounts of RNA aptamer in Reaction Buffer for 5 min at 37°C followed by addition of 20 nM T_{d31}/Cy3-P_{d18a} and 50 μM of each dNTP. (**A**) The reactions were stopped after 30 min and resolved on a polyacrylamide gel. The predicted secondary structures of each aptamer were generated by mfold. (**B**) The percent full extension was quantified for m.1.1FL (filled inverted triangle), m.1.3 (filled circle) and m.1.4 (filled square) and data points fit to one-site competition non-linear regression using GraphPad Prism 4 to calculate IC_{50}. HIV-1 RT was not susceptible to m.1.1FL (open triangle). (Errors represent data deviation from the fit).

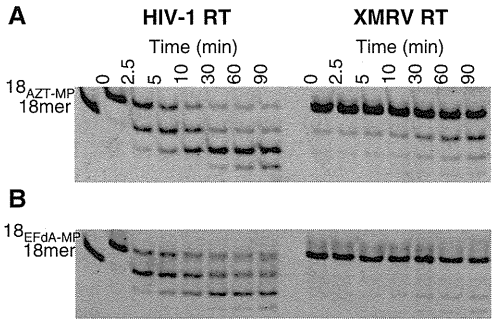

Figure 8. PPi-mediated unblocking of AZT-(A) and EFdA-(B) terminated DNA. About 20 nM of (**A**) AZT- or (**B**) EFdA-terminated T_{d31}/Cy3-P_{d18c} (T/$P_{AZT\text{-}MP}$ or T/$P_{EFdA\text{-}MP}$) was incubated with HIV-1 RT (60 nM) or XMRV RT (200 nM) in the presence of 150 μM PPi and 6 mM $MgCl_2$. Aliquots of the reactions were stopped at different time points (0–90 min) and resolved on a 15% polyacrylamide–7M urea gel as described in the 'Materials and Methods' section.

Susceptibility of mutant XMRV RTs to AZT-TP and tenofovir-DP

The HIV-1 RT mutation Q151M confers resistance to AZT by enhancing discrimination of the nucleotide analog leading to its reduced incorporation (37,66–68). Another HIV-1 RT mutation, K65R, decreases susceptibility to tenofovir (69,70). Since AZT and tenofovir are potent inhibitors of XMRV (Table 6) (54–56), we wanted to investigate whether the XMRV RT mutant equivalents of HIV Q151M and K65R (XMRV Q190M and K103R) would confer XMRV RT resistance to AZT and tenofovir. We constructed these mutant clones and tested their susceptibility to AZT and tenofovir in the same manner as wild-type XMRV RT. Interestingly, Q190M XMRV RT has a decreased susceptibility to AZT (approximately 5-fold increase in the IC_{50}). Similarly, the K103R XMRV RT mutant enzyme was less susceptible to tenofovir, increasing the IC_{50} by at least 2-fold.

Molecular model of XMRV RT

Given the significant sequence similarity between XMRV and MoMLV RTs, the resulting homology model of XMRV RT is highly similar to MoMLV RT (>1.5Å rms) and of excellent quality. Since the input structure of MoMLV RT did not contain the RNase H domain of the enzyme, the XMRV RT model is also missing this domain. The molecular model of the polymerase domain of XMRV RT is shown in Figure 9. An alignment of the MoMLV RT crystal structure (22) with the XMRV RT homology model highlights the few changes in the polymerase domain of XMRV RT. These are L29 (P in MoMLV), Q234 (L in MoMLV), R238 (Q in MoMLV) and N422 (D in MoMLV). From these, residue 422 is located in the nucleic acid binding cleft and may contribute to differences in the interactions with nucleic acid substrate. However, most of the differences between the gammaretroviral enzymes are in their RNase H domains and also in the first 30 N-terminal residues of the polymerase domain, for which we do not have structural

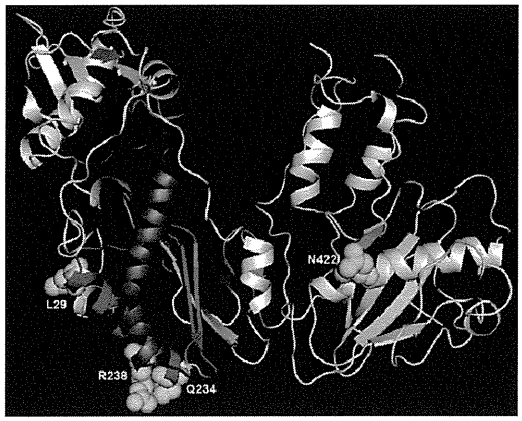

Figure 9. Molecular model of XMRV RT. Ribbons diagram of XMRV RT with the conserved polymerase Motifs color-coded: Motif A (green), B (brown), C (purple), D (red), E (orange) and F (blue). The residues that differ from MoMLV's polymerase domain are shown in ball and stick representation.

information since they were not included in the original crystal structure of MoMLV RT. The differences between XMRV RT and HIV-1 RT are very significant. Unlike the HIV enzyme, XMRV RT appears to be a monomer in solution. Moreover, alignment of the HIV-1 RT–DNA complex with XMRV RT based on their active sites at the palm subdomains shows that the thumb subdomain of XMRV RT would have to be repositioned to be able to accommodate nucleic acid.

DISCUSSION

Early studies reported the presence of XMRV in stromal cells from prostate cancer patient samples and also in CFS clinical samples. Some of the subsequent studies confirmed these findings whereas several others failed to identify XMRV in prostate cancer or in CFS patients, even when same samples were used (71). It was recently reported that human sample contamination with mouse DNA can occur frequently (17,72–74). Moreover, two coauthors from this study have recently demonstrated that XMRV is the product of recombination events between two MLV proviruses, suggesting that XMRV may not be relevant to human disease (18). Nonetheless, XMRV is still an important human retrovirus and comparisons with HIV can provide valuable insights into the fundamental mechanisms of DNA polymerization, RT inhibition and drug resistance. (75).

There is high degree of sequence similarity between the XMRV and MoMLV RTs (95% amino acid identity), and much less so with HIV-1 RT. Based on gel filtration experiments we conclude that unlike HIV-1 RT, but similar to MoMLV RT, XMRV RT exists in solution primarily as a monomer. We also included comparisons with HIV-1 RT in this study as it has been extensively studied and provides an excellent frame of reference.

We report here that there are significant differences in the DNA polymerization efficiency of the three enzymes. Although the polymerase active sites of the XMRV and MoMLV enzymes are almost identical, there is a considerable decrease in the efficiency of nucleotide incorporation by XMRV RT. Most differences in sequence are at the RNase H domain and are likely to affect polymerization by changing the positioning of DNA at the polymerase active site.

We have recently solved the crystal structure of the XMRV RNase H at high resolution (1.5Å) (pdb 3P1G) (Kirby, K.A. *et al.*, submitted for publication). We observed major differences in affinity for nucleic acid that we determined with gel-mobility shift assays and with pre-steady state kinetics. SPR experiments dissected in more detail the specific defect of XMRV RT in binding DNA. Surprisingly, XMRV RT can associate very rapidly with DNA, even more so than HIV-1 RT (Figure 1 and Table 3). However, it dissociates from DNA much faster than the HIV enzyme, resulting in an overall reduced binding affinity. A possible reason for the fast association and dissociation rates of XMRV RT may be the apparent monomeric state, which might offer facile access to the nucleic acid binding cleft, although with less contacts and lower affinity than HIV-1 RT, which is a heterodimer (76,77). This high rate of XMRV RT dissociation from DNA likely contributes to the decreased processivity observed in our study, and may have consequences in the recombination rates of this virus.

Previous sequences of XMRV from prostate cancer tumors showed low variability, suggesting that the virus may have a high fidelity of replication (1,10). Our study demonstrated that HIV-1 RT and MoMLV RT incorporated mismatched nucleotides and extended past the mismatches more efficiently than XMRV RT. Pre-steady state kinetics established that the higher overall fidelity of XMRV RT over MoMLV RT is due to a lower affinity for mismatched nucleotides. When compared to HIV-1 RT, however, XMRV RT has differs in both the nucleotide binding and incorporation steps. Nonetheless, XMRV did not have higher fidelity than a related amphotropic MLV virus or HIV-1 in a cell-based assay. It is possible that the high dNTP concentration in dividing cells can suppress mismatching events. We have previously shown (39) that as nucleotide concentrations vary in different cell lines, this can affect viral susceptibility to NRTIs, and possibly in this case also incorporation of mismatched nucleotides. Additional cell-based studies using multiple cell lines and a large panel of viruses should provide a better understanding of the relation between *in vivo* and *in vitro* fidelity.

Early studies have reported susceptibility of XMRV to some antiretrovirals that have been used in the treatment of HIV infection (53–56). In those studies the compounds were tested at the virus level. To better understand the interactions of inhibitors at their RT target level we tested here the ability of these and several more compounds to block the polymerase activity of XMRV RT. We found that two TDRTIs, EFdA-TP and ENdA-TP were very potent RT inhibitors (IC_{50}s: 0.43 μM and 0.14 μM, respectively). Unlike other NRTIs, these compounds have a 3′ OH group and are known to efficiently inhibit HIV replication by blocking translocation (32,58,78).

Preliminary experiments demonstrated that they also block XMRV RT by the same mechanism (data not shown).

In HIV, moderate resistance to EFdA is conferred by the emergence of the M184V mutation at the conserved X position of the conserved YXDD motif of the polymerase active site. Interestingly, XMRV and MoMLV RTs already have a valine (V223) at this position. This difference is likely to contribute to the better potency of EFdA against HIV-1 RT than XMRV RT or MoMLV RT (57,58). It may also contribute to the decreased ability of XMRV RT to unblock chain-terminated primers, as was also reported for M184V HIV-1 RT (79) and to the enhanced fidelity reported here for XMRV RT, which is also reminiscent of the previously reported high fidelity of M184V HIV-1 RT (80,81). Nonetheless, despite the presence of a Val in the YMDD motif of XMRV RT we found EFdA to inhibit very efficiently replication-competent or pseudotyped XMRV, with submicromolar EC_{50}s (40 and 110 nM, respectively).

Previously, highly potent aptamers were selected to inhibit MoMLV RT (60). We demonstrate here that the three aptamers we tested have varying potency against XMRV RT. Aptamer m.1.1FL was the most potent inhibitor of XMRV RT and MoMLV RT in *in vitro* assays (IC_{50} = 2 and 4 nM, respectively). The fact that XMRV and MoMLV RTs are inhibited by the same aptamers at comparable efficiencies suggests that the RT residues that are different in the two enzymes are not critical to the binding of the aptamer. In contrast, heterodimeric HIV-1 RT has a very different binding cleft and is not inhibited by these aptamers.

Tenofovir is an essential component of HIV therapies and is also a potent inhibitor of XMRV RT. HIV resistance to tenofovir is conferred by a single codon mutation (K65R). HIV-1 RT residue 65 is known to interact with the incoming dNTP or the activated tenofovir analog (tenofovir diphosphate) (82). K65R causes resistance to tenofovir by lowering the k_{pol} for the incorporation of the inhibitor into the nascent DNA. We prepared XMRV RT with the equivalent mutation, K103R, and determined that it has decreased susceptibility to tenofovir. Hence, it is possible for XMRV to develop tenofovir resistance through the same mechanism as HIV-1 RT. HIV resistance to AZT can occur by either decreased binding/incorporation or increased excision of the chain-terminating NRTI (33,83). HIV-1 RTs containing the M41L, D67N, K70R, T215Y/F, K219E/Q mutations show enhanced removal of AZT. Our experiments show that unlike wild-type HIV-1 RT, XMRV RT is not able to excise NRTI-terminated primers. Similarly, it was previously shown that MoMLV RT is not capable of unblocking chain-terminated primers (33).

In HIV, decreased binding of AZT is conferred initially in the presence of the primary Q151M mutation, followed by secondary mutations F77L, A62V, V75I and F116Y (27,47,84). XMRV RT already differs from wild-type HIV-1 RT in the first three of these residues (P104, Q113 and L115 versus A62, V75 and F77) (Table 1). We demonstrated that introducing the primary Q→M mutation at the equivalent XMRV RT site (Q190M) resulted in an enzyme with decreased susceptibility to AZT. Hence, it appears that these residues can confer AZT resistance to XMRV by reduced incorporation of nucleotide analogs, as is the case in HIV-2 (41). At this point we do not know if introduction of as yet unknown mutations could endow XMRV RT with the ability to unblock chain-terminated nucleic acids. The details of the molecular mechanism of XMRV resistance to tenofovir and AZT are under investigation.

In conclusion, our study provides detailed biochemical analysis of the mechanisms of polymerization, inhibition, fidelity, processivity and drug resistance of XMRV RT and how it compares with the closely related enzyme MoMLV RT and the more distantly related HIV-1 RT. The findings enhance our understanding of the basic mechanisms of reverse transcription.

SUPPLEMENTARY DATA

Supplementary Data are available at NAR Online.

ACKNOWLEDGEMENTS

The content of this publication does not necessarily reflect the views or policies of the Department of Health Human Services, nor does mention of trade names, commercial products or organizations imply endorsement by the U.S. Government.

FUNDING

NIH grants (AI076119, AI079801, and AI094715, to S.G.S.), (AI074389, to D.H.B.), (AI079801 to M.A.P.); NIH Bench-to-Bedside Award and the Intramural Research Program of the NIH, National Cancer Institute, Center for Cancer Research (to V.K.P); Ministry of Knowledge and Economy, Bilateral International Collaborative R&D Program, Republic of Korea; Canadian Institutes of Health Research (CIHR) and University of Missouri (to S-L.L.); amfAR Mathilde Krim Fellowship and a CIHR Fellowship (to B.M.). Funding for open access charge: NIH grants (AI076119, AI094715, AI074389, AI079801).

Conflict of interest statement. None declared.

REFERENCES

1. Urisman,A., Molinaro,R.J., Fischer,N., Plummer,S.J., Casey,G., Klein,E.A., Malathi,K., Magi-Galluzzi,C., Tubbs,R.R., Ganem,D. *et al.* (2006) Identification of a novel gammaretrovirus in prostate tumors of patients homozygous for R462Q RNASEL variant. *PLoS Pathog.*, **2**, e25.
2. Malathi,K., Dong,B., Gale,M. Jr. and Silverman,R.H. (2007) Small self-RNA generated by RNase L amplifies antiviral innate immunity. *Nature*, **448**, 816–819.
3. Arnold,R.S., Makarova,N.V., Osunkoya,A.O., Suppiah,S., Scott,T.A., Johnson,N.A., Bhosle,S.M., Liotta,D., Hunter,E., Marshall,F.F. *et al.* XMRV infection in patients with prostate cancer: novel serologic assay and correlation with PCR and FISH. *Urology*, **75**, 755–761.
4. Dong,B., Kim,S., Hong,S., Das Gupta,J., Malathi,K., Klein,E.A., Ganem,D., Derisi,J.L., Chow,S.A. and Silverman,R.H. (2007) An